High Energy Density Physics (HEDP) And Laboratory Astrophysics


X-ray: NASA/CXC/MIT/L/ Lopez et al.; INFRARED: PALOMAR; RADIO: NSF/NRAO/VLA

Assistant Professor Louise Willingale

COLLEGE OF ENGINEERING
ELECTRICAL & COMPUTER ENGINEERING
UNIVERSITY OF MICHIGAN

GPAP 2021, 11th June 2021

HEDP and Laboratory Astrophysics

- What is HEDP?
- Creating HEDP conditions in the laboratory
  - Z-pinches (pulsed power machines)
  - High-energy laser facilities
- Examples of astrophysically relevant HEDP experiments
  - Equation of state, stellar opacity, nuclear cross-sections, turbulent dynamo, instabilities (Rayleigh-Taylor, Weibel), scaled protostellar jets
- Magnetic reconnection in the laboratory
- Pair plasmas in the laboratory?

Plasma conditions

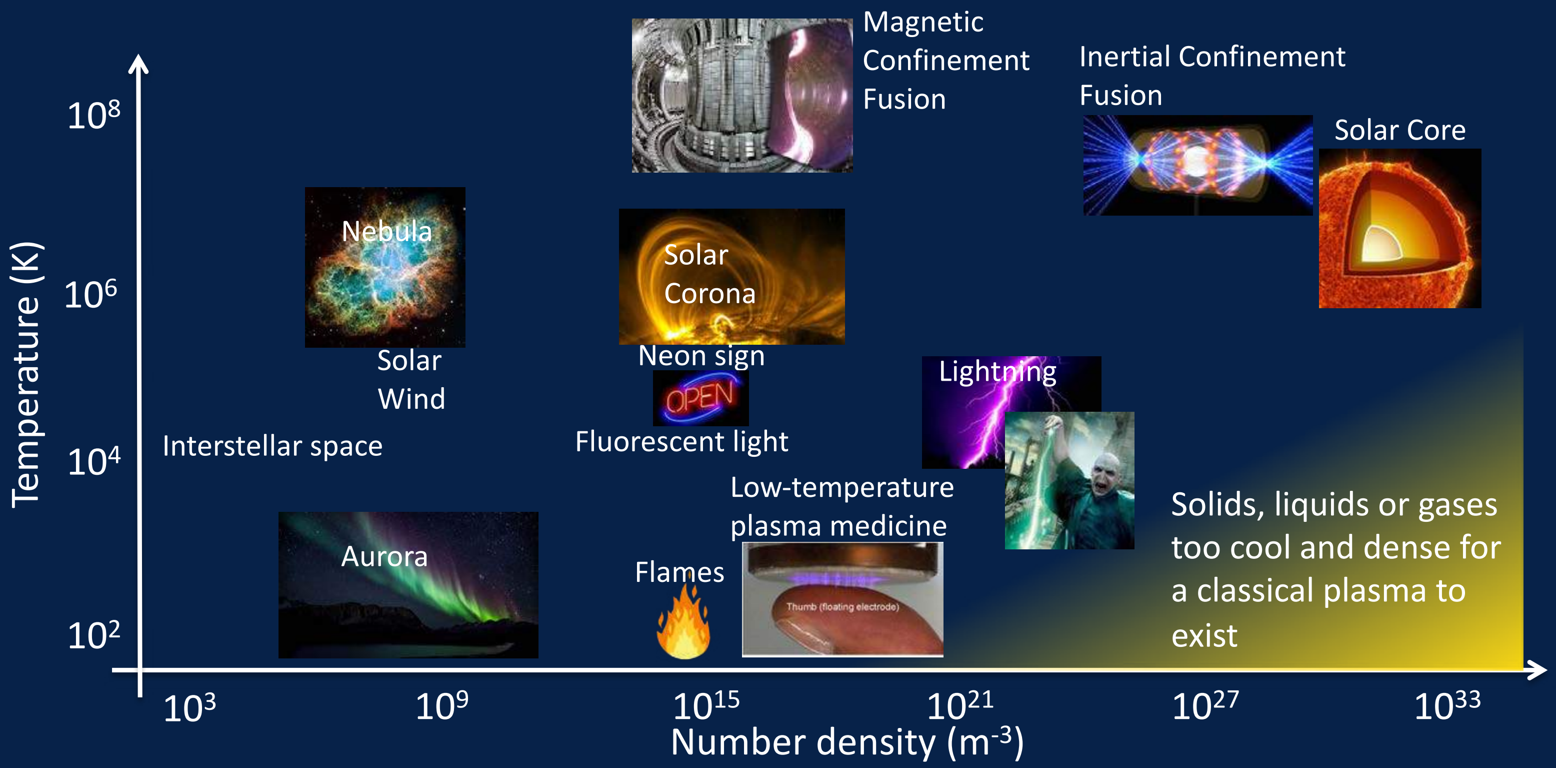

What is High Energy Density Physics (HEDP)?

- Pressure above 1 Mbar = 1 million atm

- ~ Boeing 474 on your fingertip

$$P = \frac{F}{A}$$

1000 atm →

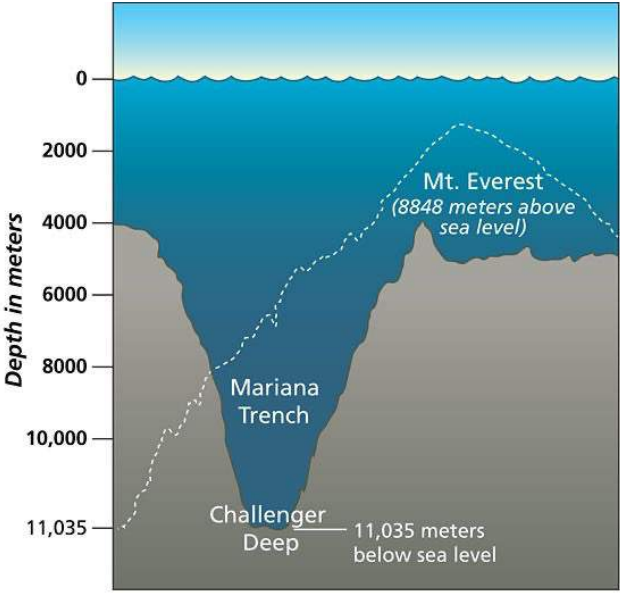

- In the ocean, reach
  - 1 atm at 10 m
  - 1 Mbar at 10^6 m (10 million meters)

What is HEDP?

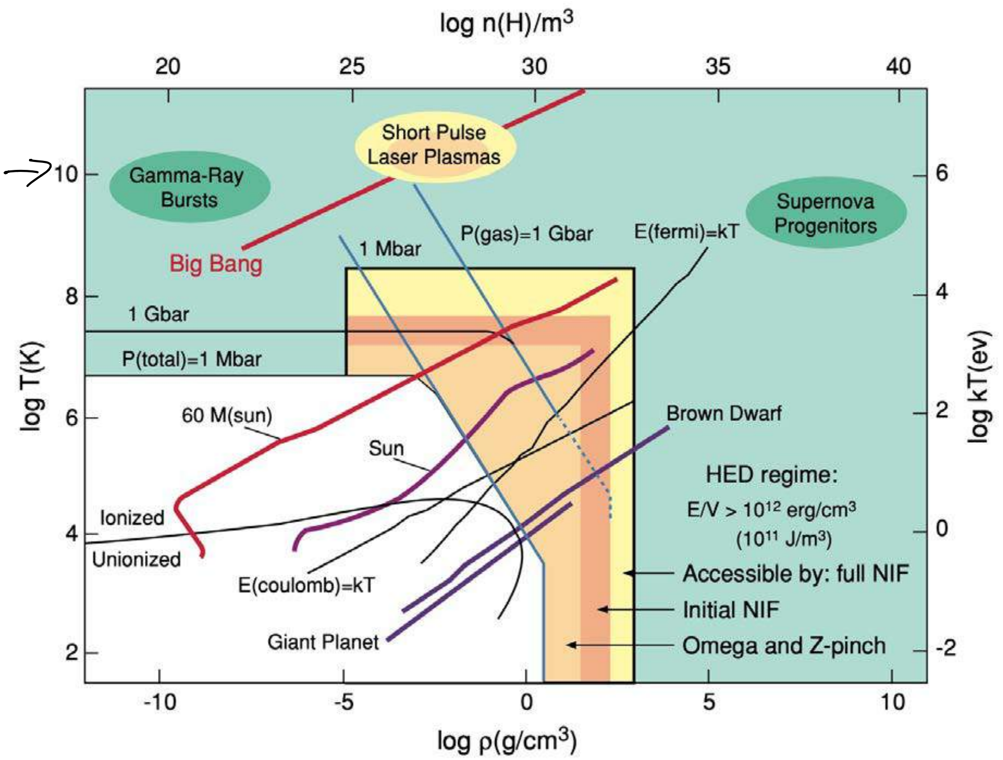

1eV ~ 10,000K

10^6eV ~ 10^{10}K

- At high n_e → pressure ionization.
- Strongly coupled: E(Coulomb) = kT → to right
- Fermi degenerate to right of E(Fermi)=kT

Frontiers in High Energy Density Physics: The X-Games of Contemporary Science, National Research Council (2003)

What is HEDP?

of e^- in Debye sphere

$$\Lambda = 4\pi n_e \lambda_D^3 \quad \text{(dimensionless)}$$

$$\lambda_D^2 = \frac{\varepsilon_0 k_B T_e}{n_e e^2} \qquad \Lambda \propto \frac{(k_B T_e)^{\frac{3}{2}}}{n_e^{\frac{1}{2}}}$$

Λ small $\longrightarrow$ non-ideal plasma

HED matter is typically a plasma, but plasma theory may not be sufficient in all regimes.

High Energy Density Physics

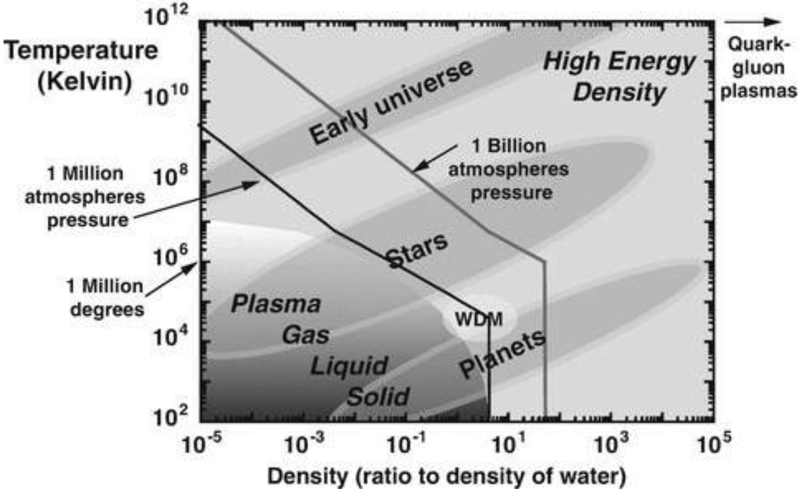

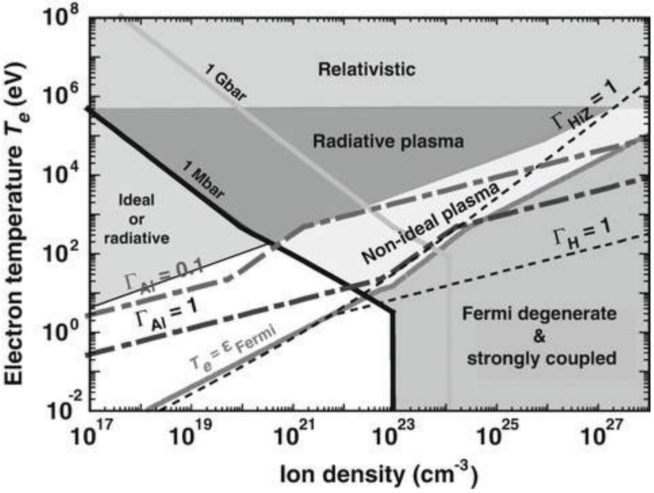

R P Drake, (2018) Introduction to High-Energy-Density Physics, Graduate Texts in Physics. Springer, Cham. https://doi.org/10.1007/978-3-319-67711-8_1

Why study HEDP?

National Nuclear Security Association

Science-based stockpile stewardship to ensure a safe, secure, and effective nuclear stockpile

Inertial Confinement Fusion Scientists

Create nuclear fusion reactions by heating and compressing a fuel

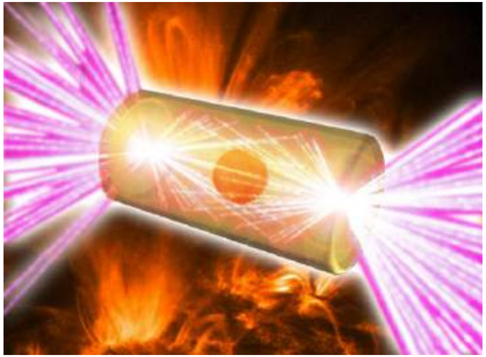

Astrophysicists

HEDP conditions found in SN explosions, SN remnants, accretion phenomena, reconnection, cosmic ray acceleration…

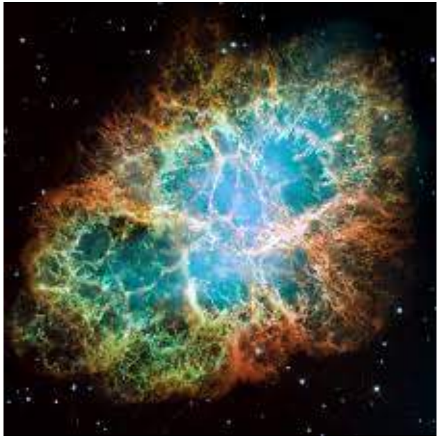

Creating HEDP conditions

High-energy, short pulse lasers

Z-pinch


NIF (LLNL)

National lab scale

Need lots of energy


Z-machine (SNL)

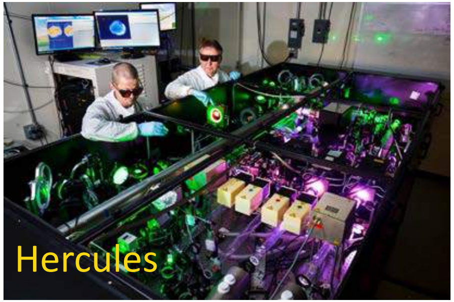
Hercules

University scale


Maize

Creating HEDP conditions: Z-pinch

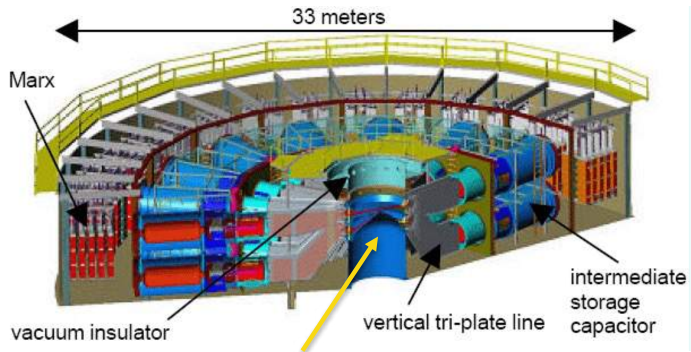

Wires are heated by current & ablate plasma
Force on plasma due to magnetic pressure (Lorentz force)

$$\bar{F} = \frac{\bar{J} \times \bar{B}}{V}$$

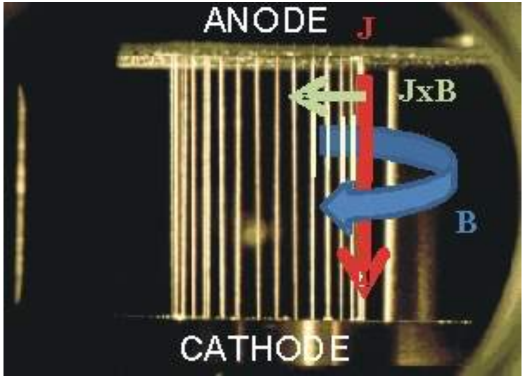

Wire array

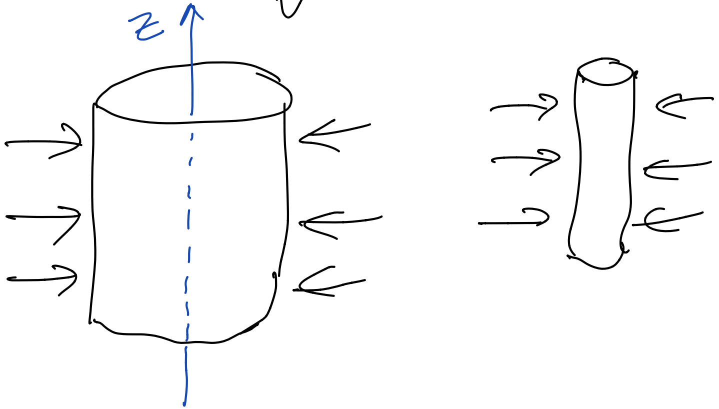

Creating HEDP conditions: Z-pinch

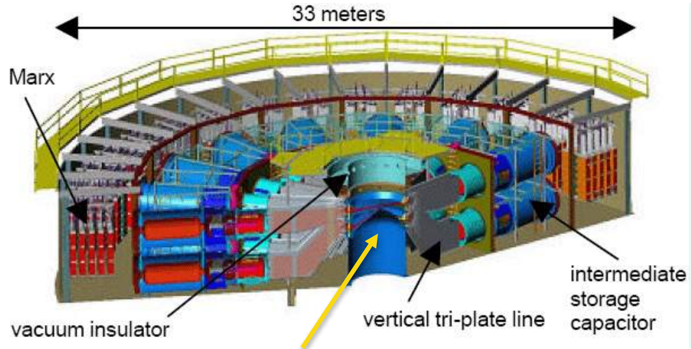

Assembles, dense, hot plasma on axis

→ source of bright x-rays

→ instabilities: sausage, kink, magneto-RT

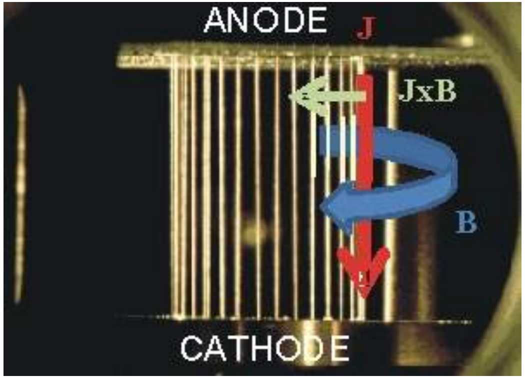

Wire array

Creating HEDP conditions: Laser pulses

NIF at LLNL

Aka “The Warp Core” on StarTrek

What can these facilities study?

…planetary interiors, equation of state, atomic processes, radiation transport, photoionization, stellar opacity, magnetic reconnection, particle acceleration, collisionless plasmas, turbulent dynamos, nuclear astrophysics, pair plasmas…

Fusion energy studies

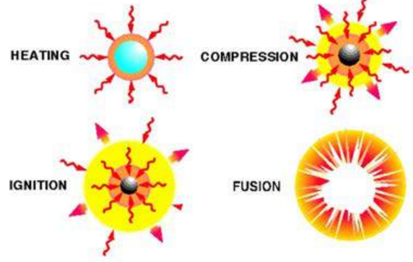

Basic plasma instabilities

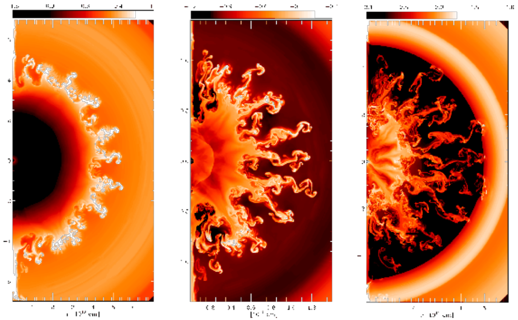

Fundamental & nuclear physics

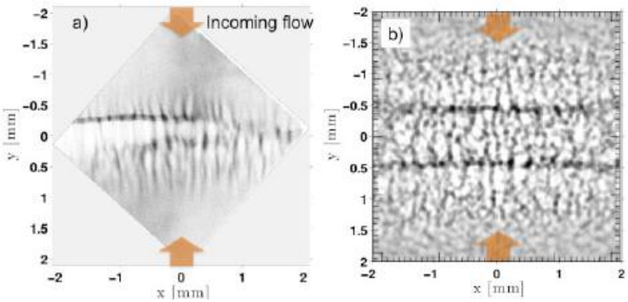

Equation of state

Target plasma density

plasma frequency $\omega_{pe} = \sqrt{\frac{n_e e^2}{\varepsilon_0 m_e}}$

Laser frequency ω_L

If $\omega_L = \omega_{pe}$

→ critical density $n_c = \frac{m_e \varepsilon_0 \omega_L^2}{e^2}$

Target plasma densities

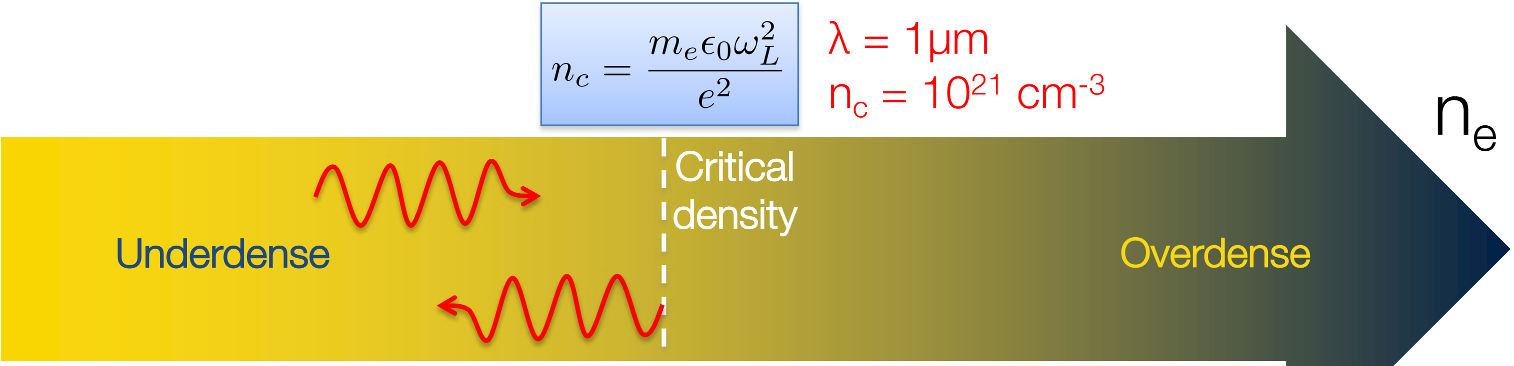

Gas Jet
$10^{18} - 10^{20}\ cm^{-3}$

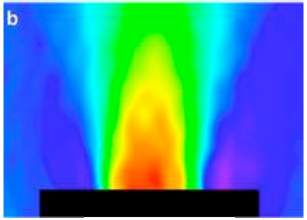

Plasma
plume

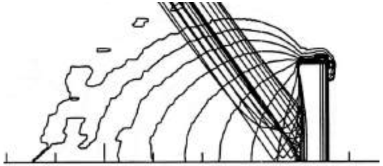

Foam
$0.9 - 30 \times 10^{21}\ cm^{-3}$

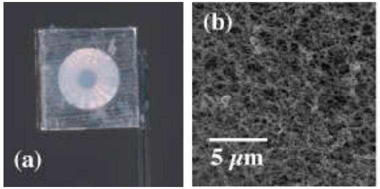

Solid foil ~ $10^{24}\ cm^{-3}$

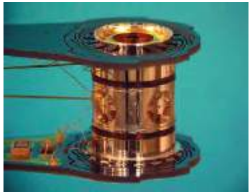

Blackbody radiation

Hot material radiates energy as photons

Blackbody radiation spectrum is given by Planck's law:

spectral radiance (power / unit solid angle / unit area normal to propagation) density of frequency, ν, radiation per unit frequency at thermal equilibrium at temperature T,

$$B_\nu(\nu, T) = \frac{2h\nu^3}{c^2}\frac{1}{e^{\frac{h\nu}{kT}}-1}$$

Planck's constant

$h = 6.6 \times 10^{-34}$ J s

$= 4.1 \times 10^{-15}$ eV.s

Blackbody radiation is isotropic

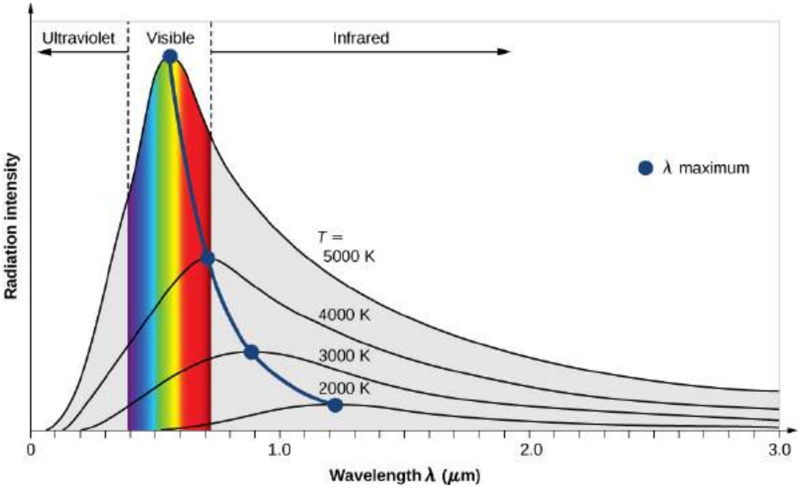

Higher T

→ Peak shifts to lower λ

→ Radiation intensity increase.

Radiation hydrodynamics

Plasma gains or loses energy & momentum through photon emission, absorption and/or scattering.

→ modify fluid energy eqn's → can alter hydrodynamics

Radiation flux is given by σT^4 (Stefan-Boltzmann Law)

If radiation flux > material energy flux

⇒ radiation dominated regime

Creating a star on Earth

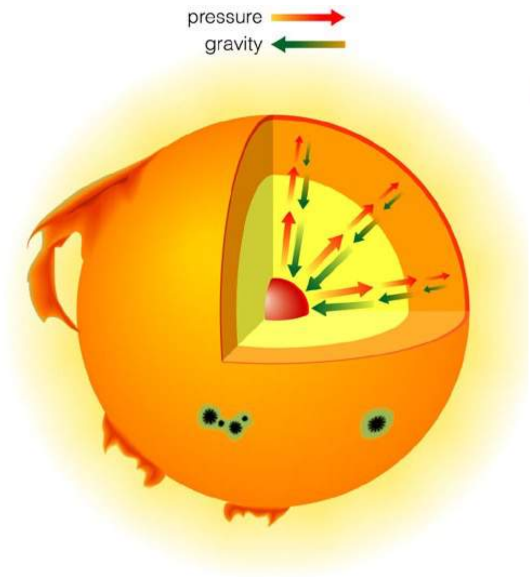

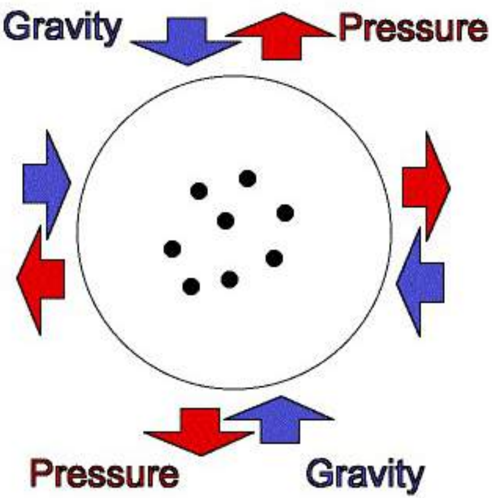

Thermonuclear fusion heats the inside of the star, creating pressure that stops the collapse and producing a long period of great stability that defines the main sequence

Star on Earth? → no gravity so need to confine fuel in another way

Inertial Confinement Fusion (ICF)

Radiation Blow-off Inward transported thermal energy

1. Laser beams or laser-produced x-rays rapidly heat the surface of the fusion target, forming a surrounding plasma envelope

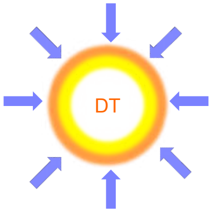

2. Fuel is compressed by the rocket-like blow off of the hot surface material

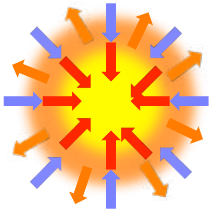

3. During the final part of the capsule implosion, the fuel core reaches 20 times the density of lead and ignites at 100,000,000°C

4. Thermonuclear burn spreads rapidly through the compressed fuel, yielding many times the input energy

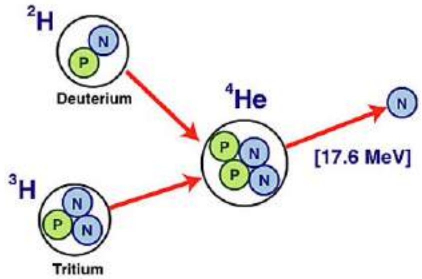

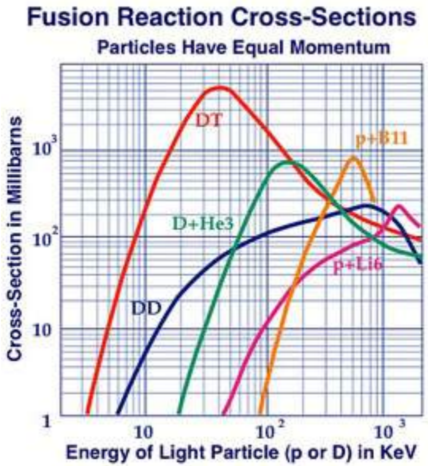

Inertial Confinement Fusion

- Hot spot conditions:
- How dense? ~x100 solid lead 600 – 800 g/cm³
- How hot? > 100 million K
- How long? ~ 10 ns

Rayleigh-Taylor instability

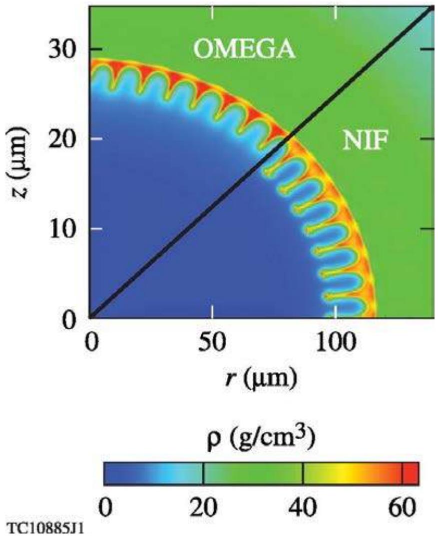

A Bose, et al., Physics of Plasmas, 22, 072702 (2015)

Equation of State

→ relates P, V, T under particular conditions

Article

A measurement of the equation of state of carbon envelopes of white dwarfs

https://doi.org/10.1038/s41586-020-2535-y
Received: 12 July 2019
Accepted: 5 May 2020
Published online: 5 August 2020
Check for updates

Andrea L. Kritcher[1✉], Damian C. Swift[1], Tilo Döppner[1], Benjamin Bachmann[1], Lorin X. Benedict[1], Gilbert W. Collins[1,2,3,4], Jonathan L. DuBois[1], Fred Elsner[5], Gilles Fontaine[6,14], Jim A. Gaffney[1], Sebastien Hamel[1], Amy Lazicki[1], Walter R. Johnson[7], Natalie Kostinski[1], Dominik Kraus[8,9], Michael J. MacDonald[1], Brian Maddox[1], Madison E. Martin[1], Paul Neumayer[10], Abbas Nikroo[1], Joseph Nilsen[1], Bruce A. Remington[1], Didier Saumon[11], Phillip A. Sterne[1], Wendi Sweet[5], Alfredo A. Correa[1], Heather D. Whitley[1], Roger W. Falcone[12] & Siegfried H. Glenzer[13]

Sun will end up as white dwarf → fuel runs out, gravity collapses material to become degenerate

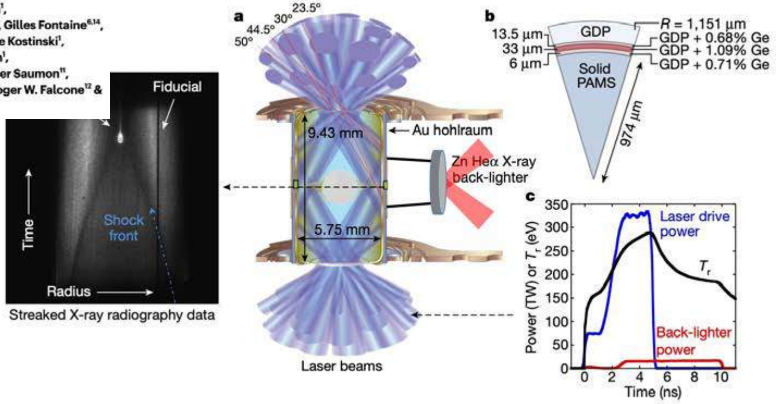

Fig. 1 | Experimental configuration. a, Schematic of the target showing laser beams incident on the inside of a gold hohlraum, a solid spherical sample inside the hohlraum, and the X-ray back-lighting configuration. **b**, Diagram of the sample configuration (that is, a portion of the sphere from **a**), showing layer thicknesses and level of Ge dopant (in atoms per cent) in the glow-discharge polymer (GDP) ablator. **c**, Laser drive (blue) and back-lighter (red) power profiles versus time. The calculated radiation temperature versus time is also shown (black curve). **d**, Streaked X-ray radiography data showing the shock front and shock flash at the core. The spatial fiducial line is used for diagnostic warp correction.

https://www.nature.com/articles/s41586-020-2535-y

Equation of State

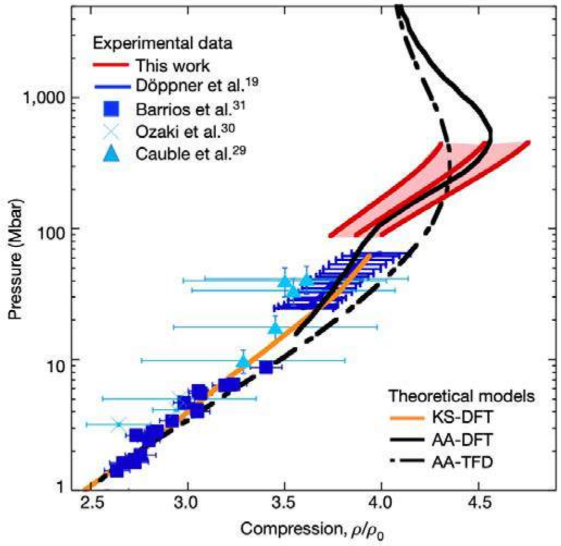

Fig. 3 | $C_9(H)_{10}$ shock Hugoniot measurements. Measured pressure versus mass density (ρ) normalized to the initial density (ρ_0) along the shock Hugoniot (red curve and shaded region). Also plotted are previous experimental data[19,29–31] and theoretical modelling of the Hugoniot using AA-TFD (black dashed curve), AA-DFT (black curve) and KS-DFT (orange curve); see text.

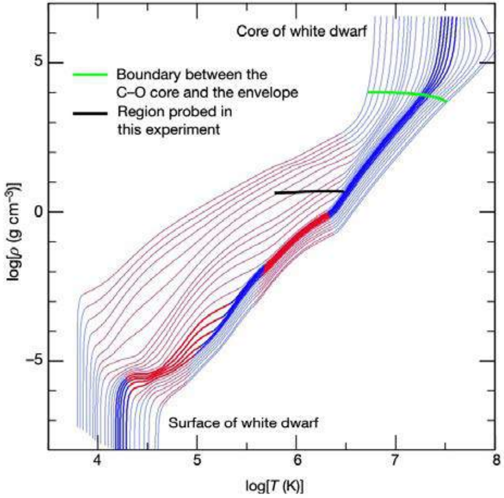

Fig. 4 | Regime of white dwarf stars accessed by measurements. Density–temperature diagram for the evolution of a white dwarf star with a mass of $0.6M_{Sun}$ composed of a carbon/oxygen core surrounded by a pure carbon envelope (M_{Sun}, mass of the Sun). The surface of the star occupies the region of the curves in the lower left and the core occupies the region of the curves in the upper right. Models start from hot and young state (right) and evolve leftward to older and colder structures, with the bold lines corresponding to hot DQ stars[3]. Convective regions in the stars are shown in red. The regime probed by the experiment is shown by the thick black line, with temperatures estimated from a model EOS[33–35].

https://www.nature.com/articles/s41586-020-2535-y

Stellar opacity

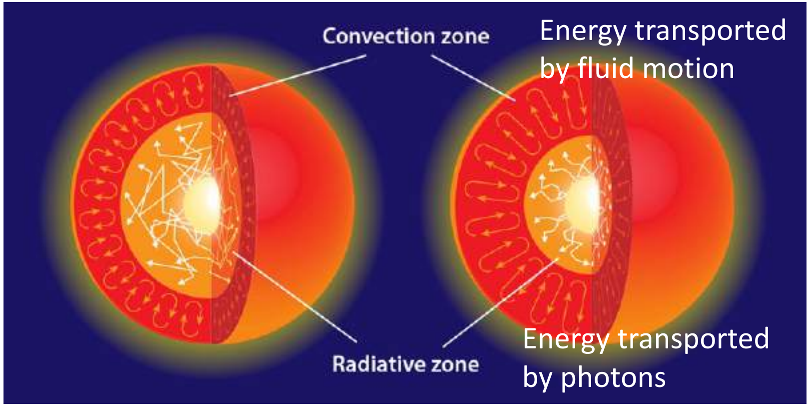

Fusion releases energy:
Particle kinetic energy or photons

Opacity $\kappa_\nu = \kappa_\nu(\rho, T, X_i)$

X_i ← local species composition

processes:
- bound-bound absorption
- bound-free absorption
- free-free absorption
- electron-scattering

→ single macroscopic quantity

κ appears in energy transport equation & is ability of a material to absorb radiation at each ν

Stellar Opacity

LETTER

doi:10.1038/nature14048

A higher-than-predicted measurement of iron opacity at solar interior temperatures

J. E. Bailey[1], T. Nagayama[1], G. P. Loisel[1], G. A. Rochau[1], C. Blancard[2], J. Colgan[3], Ph. Cosse[2], G. Faussurier[2], C. J. Fontes[3], F. Gilleron[2], I. Golovkin[4], S. B. Hansen[1], C. A. Iglesias[5], D. P. Kilcrease[3], J. J. MacFarlane[4], R. C. Mancini[6], S. N. Nahar[7], C. Orban[7], J.-C. Pain[2], A. K. Pradhan[7], M. Sherrill[3] & B. G. Wilson[5]

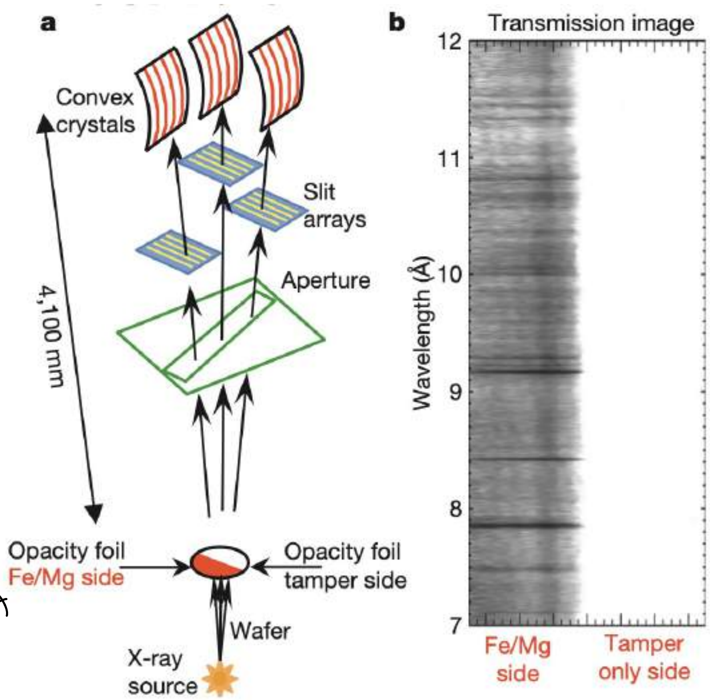

Figure 1 | Experiment diagram and example transmission image. a, Three to four spectrometers view the 'half-moon'-shaped tamped iron/magnesium sample (not to scale). Each uses multiple slits to project spatially resolved images onto a convex crystal that disperses the spectrum before recording on film (not shown). The set-up measures the unattenuated (tamper only) and the attenuated (tamper plus FeMg) spectra in the same experiment. **b,** A spatially resolved and spectrally resolved transmission image is obtained by dividing the attenuated spectral image by the unattenuated image. Darker regions correspond to higher absorption. The white portion of the image corresponds to ~100% transmission.

Sample heated to ~2 million K

https://www.nature.com/articles/nature14048

Stellar Opacity

LETTER

doi:10.1038/nature14048

A higher-than-predicted measurement of iron opacity at solar interior temperatures

J. E. Bailey[1], T. Nagayama[1], G. P. Loisel[1], G. A. Rochau[1], C. Blancard[2], J. Colgan[3], Ph. Cosse[2], G. Faussurier[2], C. J. Fontes[3], F. Gilleron[2], I. Golovkin[4], S. B. Hansen[1], C. A. Iglesias[5], D. P. Kilcrease[3], J. J. MacFarlane[4], R. C. Mancini[6], S. N. Nahar[7], C. Orban[7], J.-C. Pain[2], A. K. Pradhan[7], M. Sherrill[3] & B. G. Wilson[5]

Figure 2 | Measured iron opacity spectra at four T_e/n_e values compared with calculations. The SCRAM[23] model calculations (blue lines) account for the instrument resolution. Red lines denote the measurements and the error bars represent 1σ uncertainties. The measurements combine information from 22 separate experiments, each with three or four independent spectrometers that each record 4–6 spectra. The numbers of experiments used to infer the average opacities presented here were as follows: six for the 1.91×10^6 K/7×10^{21} cm^{-3} results; one for the 1.97×10^6 K/2×10^{22} cm^{-3} results; five for the 2.11×10^6 K/3.1×10^{22} cm^{-3} results; and ten for the 2.26×10^6 K/4×10^{22} cm^{-3} results.

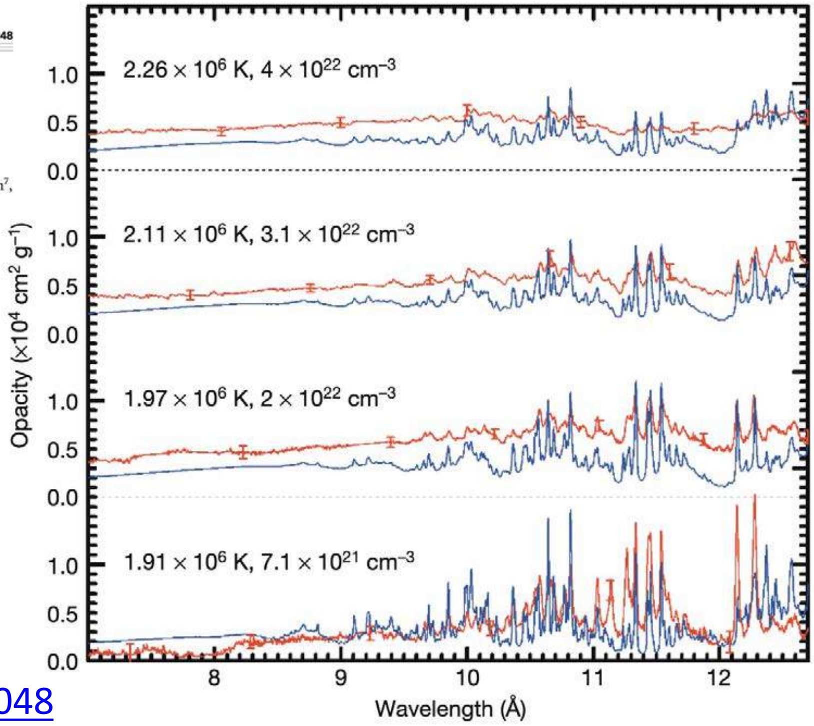

https://www.nature.com/articles/nature14048

Laboratory scales to astrophysical scales

Microscopic processes:

- Nuclear physics (reaction cross-sections)
- Atomic processes (opacity)
- Equation of state

Macroscopic plasma processes:

- Magnetic reconnection
- Instabilities: Weibel, Rayleigh-Taylor, etc
- Turbulent dynamos
- Particle acceleration
- Pair plasmas

need to consider timescales, system size & which approximations are appropriate.

Time scales

Atomic processes

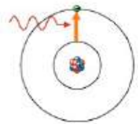

30 fs
Ti:Sapph
CPA lasers

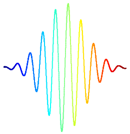

~ 1 ps
Nd:glass
CPA lasers

20 ns
NIF,
OMEGA

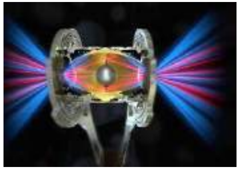

< 100 ns
Z-pinch
currents

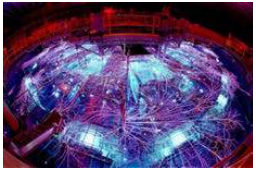

attosecond	femtosecond	picosecond	nanosecond
as	fs	ps	ns
10^{-18} s	10^{-15} s	10^{-12} s	10^{-9} s

Laboratory scales to astrophysical scales

Identify the relevant dimensionless parameters for the system of interest

eg. * Plasma beta, $\beta = \frac{\text{plasma pressure}}{\text{magnetic pressure}} = \frac{n_e k_B T_e}{B^2/2\mu_0}$

* Lundquist number, $S = \frac{L V_A}{\eta}$

Compares Alfvén crossing timescale across system (size L) to timescale of resistive diffusion (η = magnetic diffusivity)

* Reynolds number $R_e = \frac{uL}{\nu}$

Low R_e → laminar flow

High R_e → turbulent flow

u = characteristic velocity

ν = kinematic viscosity

NRL plasma physics formulary

Plasma instabilities: Rayleigh-Taylor

nature COMMUNICATIONS

ARTICLE

DOI: 10.1038/s41467-018-03548-7 OPEN

How high energy fluxes may affect Rayleigh–Taylor instability growth in young supernova remnants

C.C. Kuranz[1], H.-S. Park[2], C.M. Huntington[2], A.R. Miles[2], B.A. Remington[2], T. Plewa[3], M.R. Trantham[1], H.F. Robey[2], D. Shvarts[4,5], A. Shimony[4,5], K. Raman[2], S. MacLaren[2], W.C. Wan[1,6], F.W. Doss[6], J. Kline[6], K.A. Flippo[6], G. Malamud[1,5], T.A. Handy[1], S. Prisbrey[2], C.M. Krauland[7], S.R. Klein[1], E.C. Harding[8], R. Wallace[2], M. J. Grosskopf[9], D.C. Marion[1], D. Kalantar[2], E. Giraldez[7] & R.P. Drake[1]

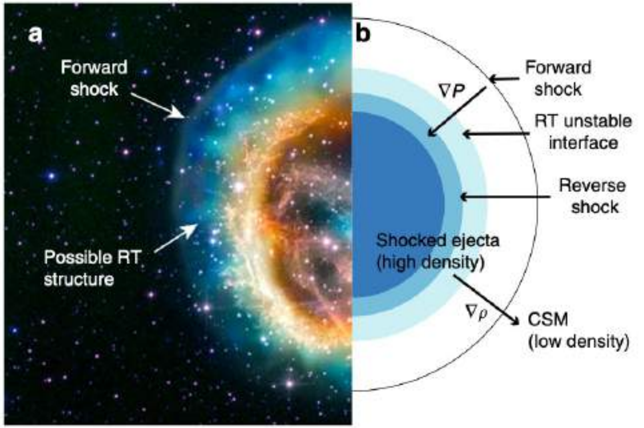

Fig. 4 Image of supernova remnant. **a** False-color image of SNR E0102.2-72. This object is believed to result from a core-collapse supernova about 1000 years ago. One can see the edge of the forward shock. The modulated boundary within it might be structuring of the ejecta-CSM interface produced by RT. The brighter, inner colors are attributed to emission from the higher-Z, interior portions of the ejecta. We credit John Hughes of Rutgers University with having called the potential connection to RT to our attention. Image credit: X-ray (NASA/CXC/MIT/D. Dewey et al. and NASA/CXC/SAO/J. DePasquale); Optical (NASA/STScI). **b** Schematic (size and shape not to scale) of inner structures of the supernova that creates the opposing density and pressure gradients to create an RT unstable interface

https://www.nature.com/articles/s41467-018-03548-7

Plasma instabilities: Rayleigh-Taylor

Fig. 1 Experimental target and radiographs. **a** NIF target schematic with laser beams incident on the gold hohlraum to create the X-ray drive and on the large-area backlighter to create the diagnostic X-ray source. Attached to the hohlraum is a plastic shock tube. The soft X-rays from the hohlraum create a shock wave in the plastic layer inside the shock tube **b**, which decays into a blast wave before crossing the unstable interface and entering the foam. The diagnostic X-ray source creates radiographs by being preferentially absorbed by a tracer layer in center of the plastic. **c**, **d** X-ray radiographs of the experiment. Here, the plasma flows upward and the dark fingers are due to RT instability growth. The color bar indicates the relative transmission for **c** the high-flux case at $t = 13$ ns and **d** the low-flux case taken at $t = 34$ ns. The two experiments have similar RT growth factors, as described in the text

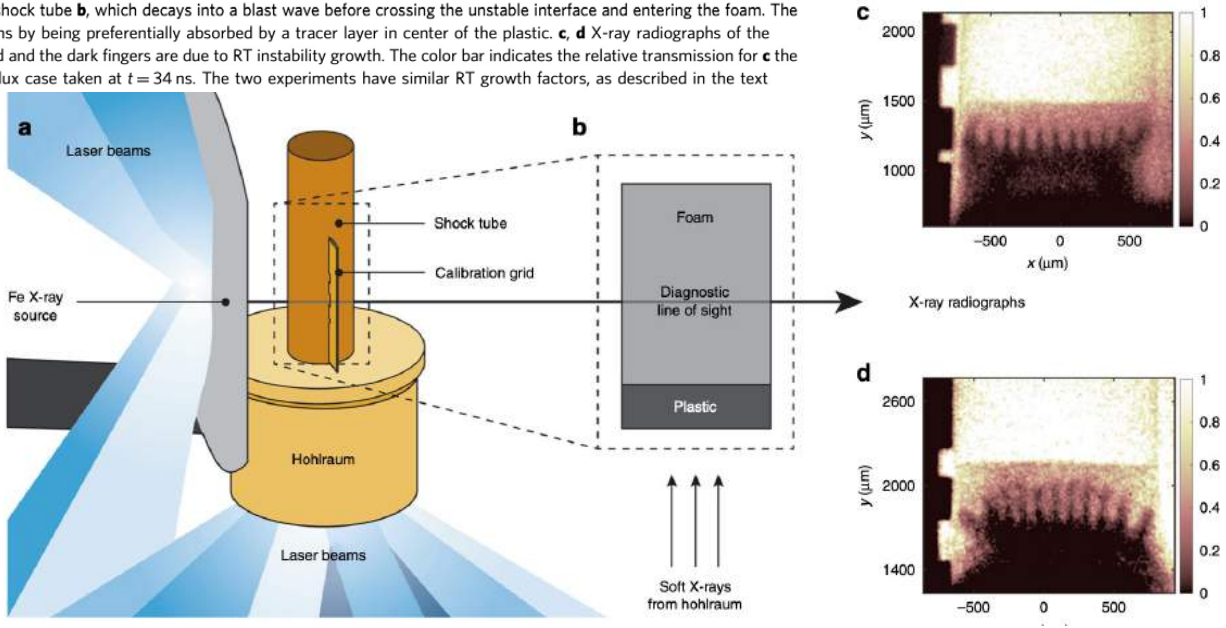

https://www.nature.com/articles/s41467-018-03548-7

Plasma instabilities: Rayleigh-Taylor

Scale Parameter	SN1993J	NIF experiment
Intershock distance L (cm)	$2.8 \times 10^{14} t_{\mathrm{yr}}^{0.95}$	0.02
Shock separation speed U (cm^{-1})	$3.0 \times 10^{8} t_{\mathrm{yr}}^{-0.046}$	6.8×10^{6}
Ejecta density at RS (g cm^{-3})	$3.4 \times 10^{-19} t_{\mathrm{yr}}^{-1.6}$	0.026
SEL Density (g cm^{-3})	$1.4 \times 10^{-16} t_{\mathrm{yr}}^{-1.6}$	0.5
SCSM Density (g cm^{-3})	$9 \times 10^{-19} t_{\mathrm{yr}}^{-1.6}$	0.18
SEL Temperature (eV)	$3800 t_{yr}^{-0.092}$	20
SCSM Temperature (eV)	$7.8 \times 10^{5} t_{\mathrm{yr}}^{-0.092}$	80
RS Velocity (km s^{-1})	$1.7 \times 10^{4} t_{\mathrm{yr}}^{-0.046}$	35
FS Velocity (km s^{-1})	$2 \times 10^{4} t_{\mathrm{yr}}^{-0.046}$	170
Z	1	2
A	1	20

https://www.nature.com/articles/s41467-018-03548-7

CC Kuranz, University of Michigan

Plasma instabilities: Rayleigh-Taylor

Table 1 Dimensionless parameters and their physical meaning

Dimensionless number	SN1993J	NIF experiment	Physical meaning
λ_c/L	$\sim 10^{-4}$	$\sim 10^{-8}$	Highly collisional
Re	$\sim 10^{6}$	$\sim 10^{7}$	Negligible viscosity
Energy flux ratio R	$\sim 10^{3}$	~ 2	Energy fluxes are important

Both SN1993J (at 0.1 years) and the laboratory experiment have characteristic length $L \gg \lambda_c$, the mean free path for ion-ion collisions, in their denser shocked layers. They also have large Reynolds number, $\mathrm{Re} = UL/\nu$, where U is the characteristic velocity and ν is the kinematic viscosity. The text discusses the energy flux ratio R

https://www.nature.com/articles/s41467-018-03548-7

Biermann battery field generation

Ohm's law $\bar{E} = -\bar{u}\times\bar{B} + \frac{\bar{j}}{\sigma} + \frac{1}{en_e}\bar{j}\times\bar{B} - \frac{1}{en_e}\nabla p_e$

↑ electron pressure term.

$$\frac{\partial \bar{B}}{\partial t} = -\nabla\times\bar{E} = \frac{1}{e}\nabla\times\left(\frac{\nabla p_e}{n_e}\right)$$

Consider an ideal gas $p_e = n_e k_B T_e$

$$\frac{\partial \bar{B}}{\partial t} = -\frac{k_B}{en_e}\nabla n_e \times \nabla T_e$$

Biermann battery

Turbulent dynamo

nature COMMUNICATIONS

ARTICLE

DOI: 10.1038/s41467-018-02953-2 OPEN

Laboratory evidence of dynamo amplification of magnetic fields in a turbulent plasma

P. Tzeferacos[1,2], A. Rigby[1], A. F. A. Bott[1], A.R. Bell[1], R. Bingham[3,4], A. Casner[5], F. Cattaneo[2], E.M. Churazov[6,7], J. Emig[8], F. Fiuza[9], C.B. Forest[10], J. Foster[11], C. Graziani[2], J. Katz[12], M. Koenig[13], C.-K. Li[14], J. Meinecke[1], R. Petrasso[14], H.-S. Park[8], B.A. Remington[8], J.S. Ross[8], D. Ryu[15], D. Ryutov[8], T.G. White[1], B. Reville[16], F. Miniati[17], A.A. Schekochihin[1], D.Q. Lamb[2], D.H. Froula[12] & G. Gregori[1,2]

Abstract

Magnetic fields are ubiquitous in the Universe. The energy density of these fields is typically comparable to the energy density of the fluid motions of the plasma in which they are embedded, making magnetic fields essential players in the dynamics of the luminous matter. The standard theoretical model for the origin of these strong magnetic fields is through the amplification of tiny seed fields via turbulent dynamo to the level consistent with current observations. However, experimental demonstration of the turbulent dynamo mechanism has remained elusive, since it requires plasma conditions that are extremely hard to re-create in terrestrial laboratories. Here we demonstrate, using laser-produced colliding plasma flows, that turbulence is indeed capable of rapidly amplifying seed fields to near equipartition with the turbulent fluid motions. These results support the notion that turbulent dynamo is a viable mechanism responsible for the observed present-day magnetization.

https://www.nature.com/articles/s41467-018-02953-2

Turbulent dynamo

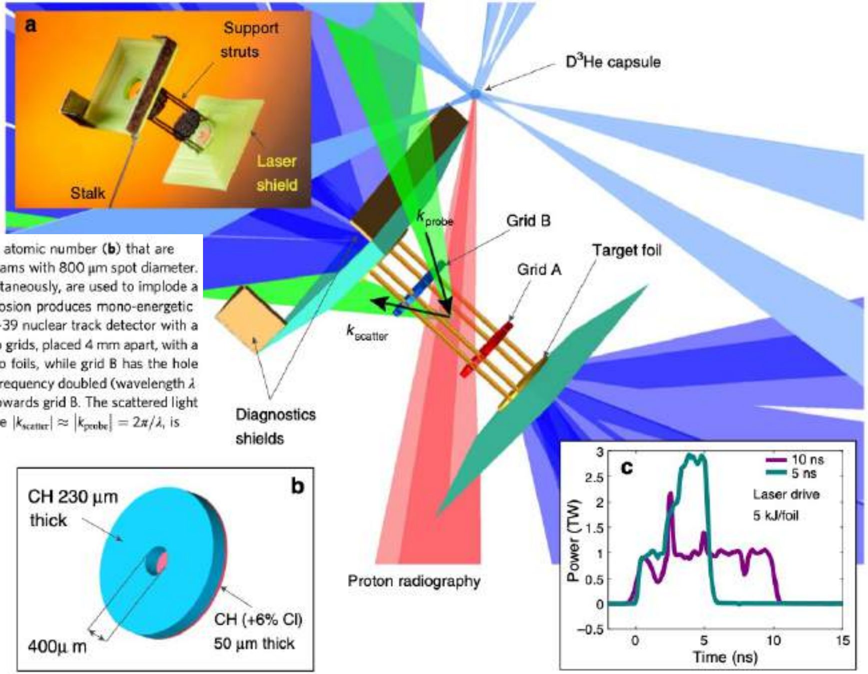

Fig. 1 Experimental configuration. The main target (see photo in **a**) consists of two CH foils doped with 6% chlorine in atomic number (**b**) that are separated by 8 mm. Each foil is illuminated by ten 500 J, 1 ns pulse length, frequency tripled (351 nm wavelength) laser beams with 800 µm spot diameter. The beams are stacked in time to achieve the two pulse profiles shown in **c**. An additional set of 17 beams, all fired simultaneously, are used to implode a 420 µm diameter capsule consisting of a 2-µm-thick SiO_2 shell filled with D_2 gas at 6 atm and ^{3}He at 12 atm. The implosion produces mono-energetic protons at 3.3 and 15 MeV with ~40 µm diameter source size, which traverse the plasma and are then collected by a CR-39 nuclear track detector with a total magnification factor of 28. The plasma expansion towards the center of the target is perturbed by the presence of two grids, placed 4 mm apart, with a 300 µm hole width and 300 µm hole spacing. Grid A has the central hole aligned on the center axis connecting the two foils, while grid B has the hole pattern shifted so that the central axis crosses the middle point between two holes. Thomson scattering uses a 30 J, 1 ns, frequency doubled (wavelength λ = 526.5 nm) laser beam to probe the plasma on the axis of the flow, 400 µm from the center and in a 50 µm focal spot, towards grid B. The scattered light is collected with 63° scattering angle and the geometry is such that the scattering wavenumber $k = k_{scatter} - k_{probe}$, where $|k_{scatter}| \approx |k_{probe}| = 2\pi/\lambda$, is parallel to the axis of the flow

https://www.nature.com/articles/s41467-018-02953-2

Turbulent dynamo

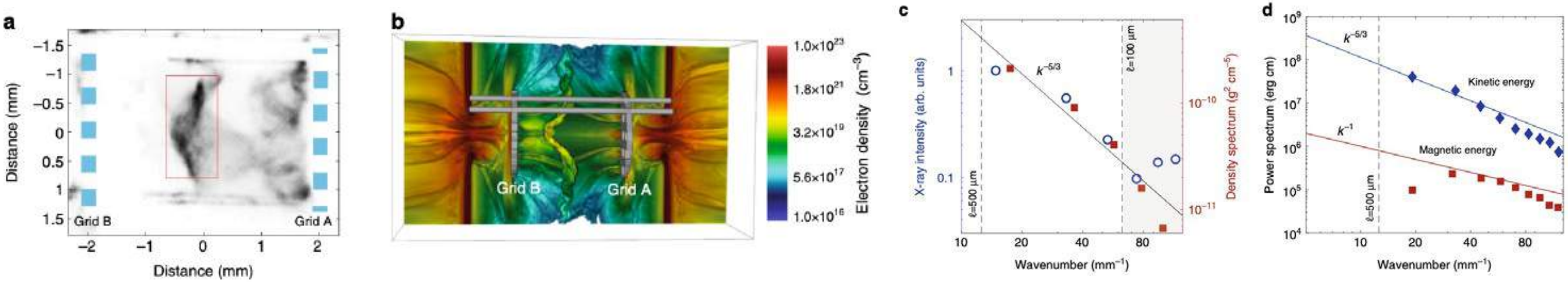

Fig. 2 Characterization of the plasma turbulence. **a** X-ray pinhole image of the colliding flows at $t = 35$ ns after the laser drive, using the 5 ns pulse profile. The image was recorded onto a framing camera with ~1 ns gate width and filtered with 0.5 μm C_2H_4 and 0.15 μm Al. The pinhole diameter is 50 μm. **b** Rendering of the electron density from three-dimensional FLASH simulations at $t = 35$ ns. **c** The open blue circles give the power spectrum of the X-ray emission from the collision region, defined by the rectangular region shown in panel **a**. The power spectrum has been filtered to remove edge effects and image defects. Details of this procedure are given in Supplementary Methods. The shaded region at high wavenumbers is dominated by noise. The spectrum of the density fluctuations, as obtained from FLASH simulations in the turbulent region, is shown with red squares. **d** Blue diamonds: power spectrum of the kinetic energy from FLASH simulations. Red squares: power spectrum of magnetic energy from FLASH simulations. The simulated magnetic energy spectrum is considerably shallower than the Kolmogorov-like kinetic energy spectrum, as predicted by ref. [23] and other studies in the Pm <1 regime (see text)

https://www.nature.com/articles/s41467-018-02953-2

Plasma instabilities: Weibel

Figure 1: Composite X-ray (blue and green), infrared (yellow and orange) and radio (pink) image of supernova remnant W49B, which is believed to be the result of a gamma-ray burst that took place a few thousand years ago in the Milky Way.

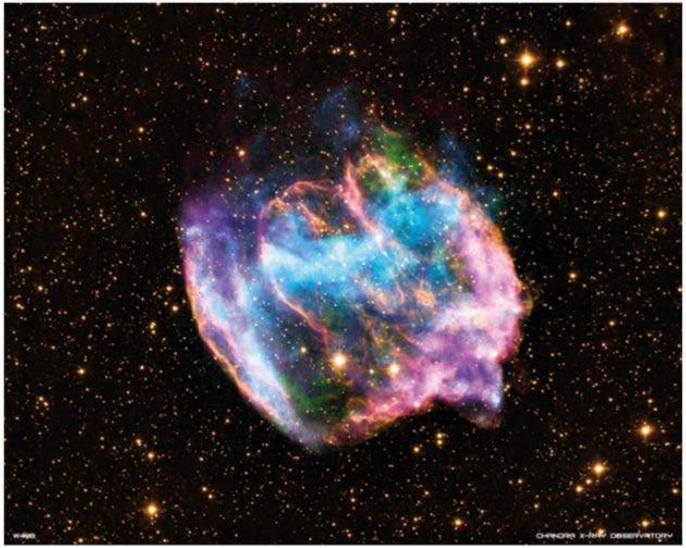

© X-ray: NASA/CXC/MIT/L.Lopez *et al.*; INFRARED: PALOMAR; RADIO: NSF/NRAO/VLA

The Weibel instability is one candidate mechanism for the generation of sufficiently strong fields to create a collisionless shock.

Francisco Suzuki-Vidal, Nature Physics, volume 11, pages 98–99 (2015)

Plasma instabilities: Weibel

nature physics
LETTERS
PUBLISHED ONLINE: 19 JANUARY 2015 | DOI: 10.1038/NPHYS3178

Observation of magnetic field generation via the Weibel instability in interpenetrating plasma flows

C. M. Huntington[1]*, F. Fiuza[1], J. S. Ross[1], A. B. Zylstra[2], R. P. Drake[3], D. H. Froula[4], G. Gregori[5], N. L. Kugland[6], C. C. Kuranz[3], M. C. Levy[1], C. K. Li[2], J. Meinecke[5], T. Morita[7], R. Petrasso[2], C. Plechaty[1], B. A. Remington[1], D. D. Ryutov[1], Y. Sakawa[7], A. Spitkovsky[8], H. Takabe[7] and H.-S. Park[1]

No initial B-field ; plasma w/ anisotropic velocity → causes plasma to bunch up & form current filaments → strong B-fields.

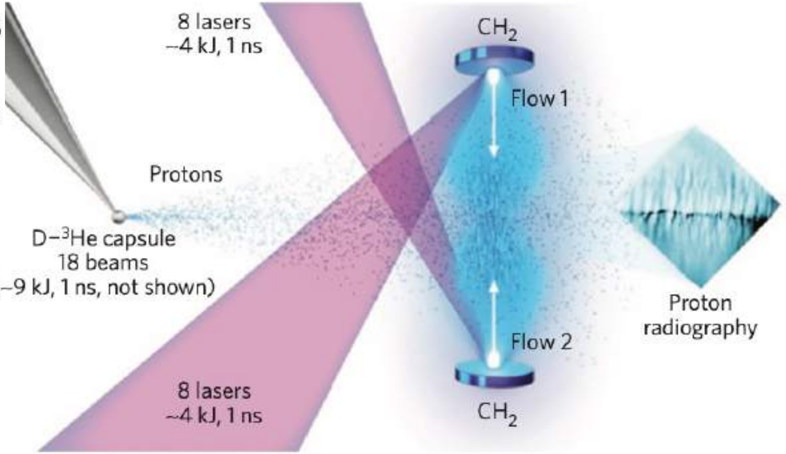

Figure 1 | Experimental configuration to generate opposing plasma flows probed by D-^{3}He protons. The experiment consists of a pair of (CH_2) plastic foils of diameter 2 mm and thickness 500 μm, oriented face-on and separated by 8 mm. Each was irradiated with eight overlapped laser beams, delivering ~4 kJ of 351 nm laser energy in a 1 ns square pulse. Distributed phase plates were used to produce super-Gaussian laser spots with focal spot diameters of 250 μm on the target surface. After a delay, the proton probe was created by laser-compressing a thin-walled SiO_2 capsule. The capsule was filled with a 1:1 mixture of deuterium (D) and ^{3}helium (^{3}He) at a total pressure of 18 atm. At peak compression (10^{23} cm^{-3}) protons are produced quasi-isotropically at energies of 3.0 and 14.7 MeV. The protons were detected using a CR39 nuclear track detector positioned on the midplane of the CH_2 target foils, such that the protons traverse the central interaction region as shown.

https://www.nature.com/articles/nphys3178

Plasma instabilities: Weibel

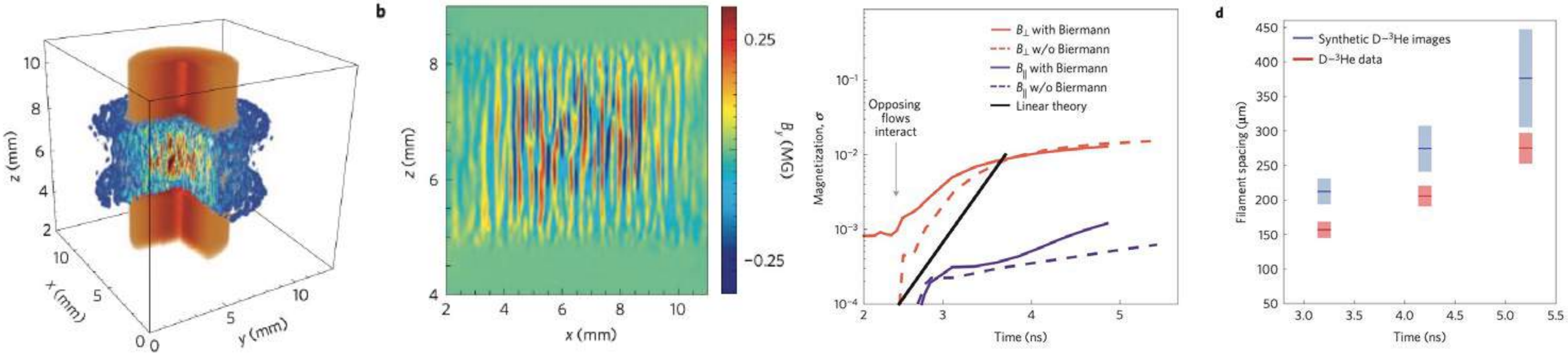

Figure 3 | Temporal evolution of magnetic field magnitude from simulation and field structure from experimental images. a, 3D OSIRIS simulation of the system after 1 ns of interaction between the counter-streaming 1,900 km s^{-1} plasma flows (approximately 3 ns after the experimental drive laser pulse; flows enter from top and bottom). Magnetic fields are shown qualitatively in the blue/red colour scale, with electron density in orange. **b**, Magnetic field slice (transverse magnetic field component B_y) along the *y*-axis midplane, at the same time, illustrating the presence of strong filaments associated with the Weibel instability. **c**, Plasma magnetization, σ, as a function of time. When the flows are initiated with zero initial magnetic field (dashed lines) the magnetizations remain at zero until the flows begin interacting, between 2 and 3 ns. When initial toroidal fields are included consistent with the Biermann-battery mechanism, the perpendicular magnetization is ~0.1% before the flows interact (solid coloured lines). In both cases the magnetic energy associated with Weibel instability increases sharply after the flows interact, increasing σ by a factor greater than ten in several ns. The magnetization due to the ion Weibel instability, growing at the theoretical linear growth rate, is shown in solid black. This calculation shows that the Weibel-generated magnetization becomes the dominant contribution to the overall magnetization of the system. **d**, Measurement of the mean separation between filaments in experimental proton radiographs (red) and synthetic proton images from 3D PIC simulations (blue). The filament spacing approximately doubles over the 2 ns of observation. Note that time is experimental time, measured with respect to the beginning of the drive laser.

https://www.nature.com/articles/nphys3178

Laser-plasma generated magnetic fields

Nanosecond pulses, $I \sim 10^{14}$ Wcm^{-2}
$B \sim 1$ MG
$v_B \sim 10^5$ ms^{-1}

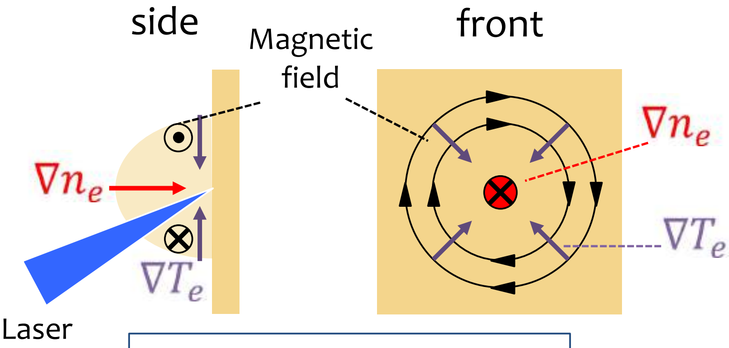

$$\frac{\partial \mathbf{B}}{\partial t} = \frac{k_B}{e n_e} \nabla T_e \times \nabla n_e$$

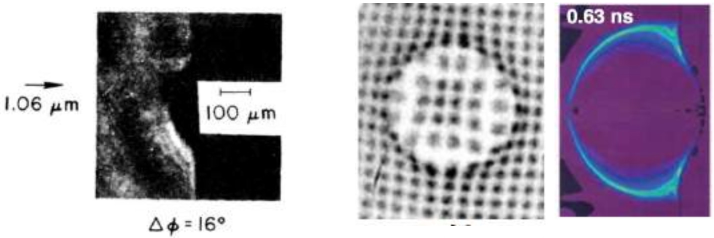

JA Stamper and BH Ripen, PRL, 34, 138 (1975)

CK Li, et al., PRL, 97, 255001 (2006)

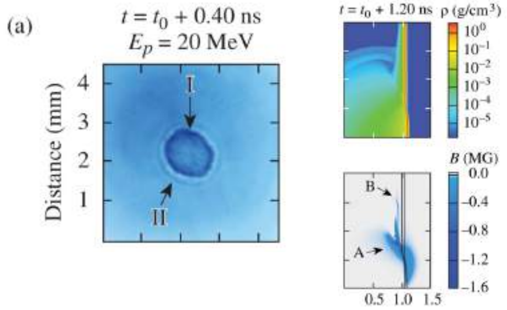

L. Gao et al. PRL, 114, 215003 (2015)

Laser driven magnetic reconnection

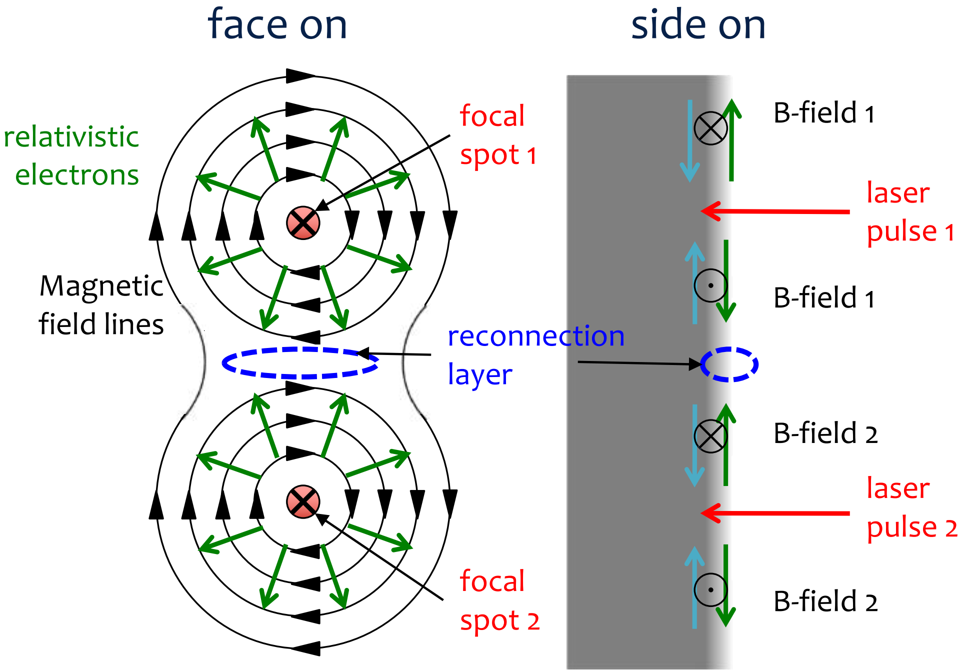

Driven reconnection.

Difficult to define dimensionless parameters because of steep gradients in n_e, B, etc

$S \sim 100 - 1000$

$d_i \sim 40\mu m$

c.f. current sheet width.

Z-pinch driven magnetic reconnection

PRL 118, 085001 (2017) PHYSICAL REVIEW LETTERS week ending 24 FEBRUARY 2017

Anomalous Heating and Plasmoid Formation in a Driven Magnetic Reconnection Experiment

J. D. Hare,[1,*] L. Suttle,[1] S. V. Lebedev,[1,†] N. F. Loureiro,[2] A. Ciardi,[3] G. C. Burdiak,[1] J. P. Chittenden,[1] T. Clayson,[1] C. Garcia,[1] N. Niasse,[1] T. Robinson,[1] R. A. Smith,[1] N. Stuart,[1] F. Suzuki-Vidal,[1] G. F. Swadling,[1,‡] J. Ma,[4] J. Wu,[5] and Q. Yang[6]

The colliding plasma flows were supersonic ($M_s \sim 1.6$) but sub-Alfvénic ($M_A \sim 0.7$), and therefore the thermal and dynamic plasma betas (ratio of the thermal or ram pressure to the magnetic pressure) are close to unity ($\beta_{th} \sim 0.7$, $\beta_{dyn} \sim 0.9$). These parameters are significantly different from those found both in magnetically driven experiments, such as MRX, and in laser driven experiments,

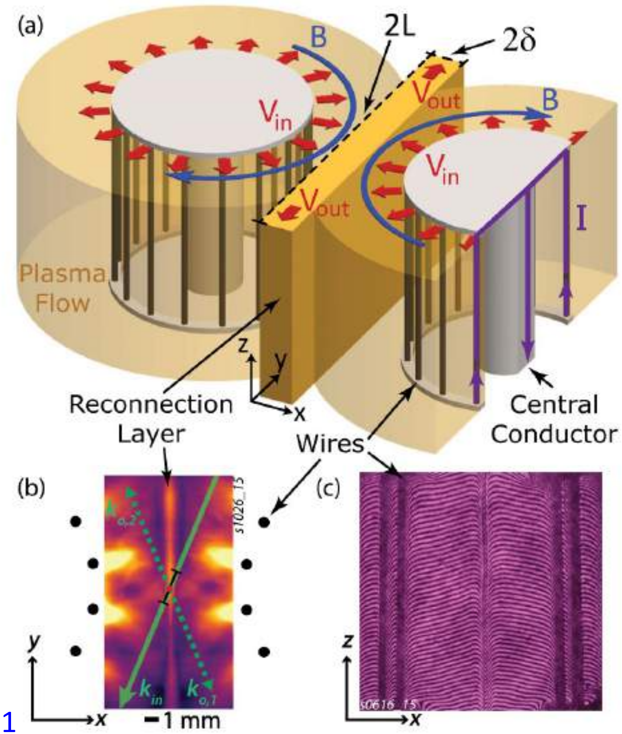

FIG. 1. (a) Experimental setup with the geometry of the reconnection layer. The cutaway on the right array shows the current path. (b) Top view with density map (taken at $t = 272$ ns after current start) and Thomson scattering vectors. (c) Side view interferogram.

https://journals.aps.org/prl/abstract/10.1103/PhysRevLett.118.085001

Z-pinch driven magnetic reconnection

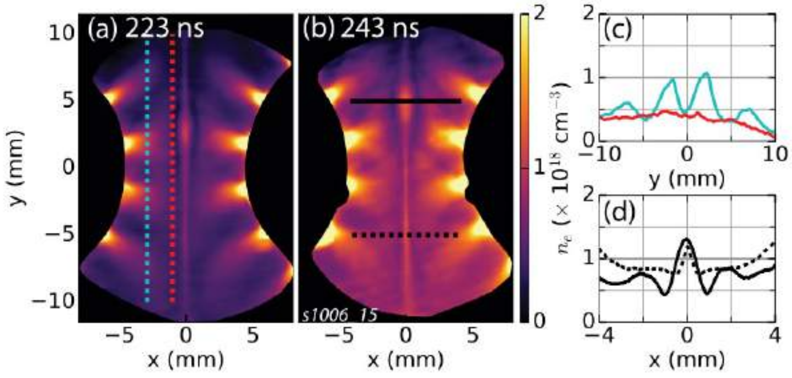

FIG. 2. Electron density maps from laser interferometry, both from the same shot. (a) At 223 ns after current start. (b) At 243 ns after current start. In both (a) and (b) there is an obvious region of enhanced density (a "plasmoid") inside the reconnection layer. (c) Lineouts of electron density; x positions shown in (a). (d) Lineouts of electron density across the reconnection layer; y positions shown in (b).

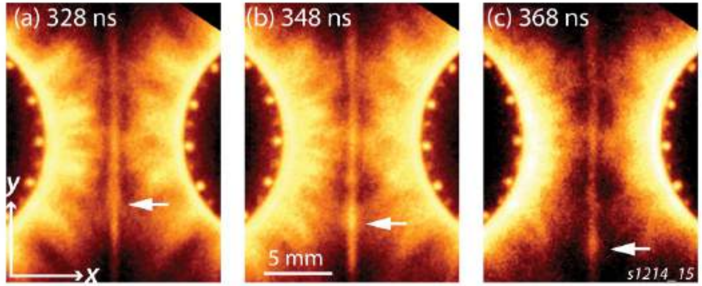

FIG. 5. Plasmoid formation and dynamics in three optical self-emission images from the same experiment: 5 ns exposure, 20 ns between frames. The location of one plasmoid in each frame is indicated with a white arrow.

https://journals.aps.org/prl/abstract/10.1103/PhysRevLett.118.085001

Creating HEDP conditions: Laser pulses

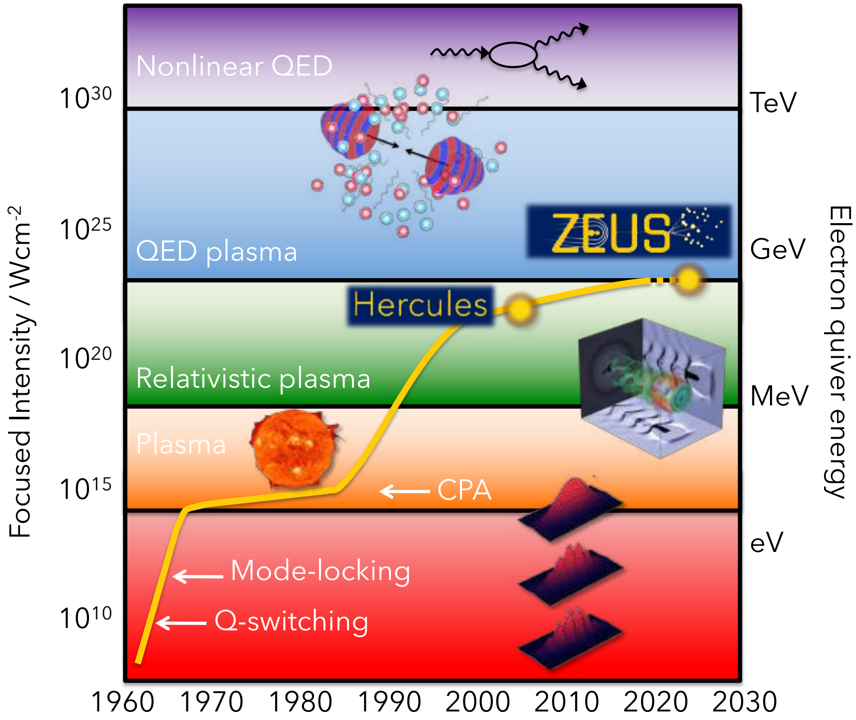

2018 Nobel prize for Physics awarded for CPA development

Chirped Pulse Amplification (CPA)

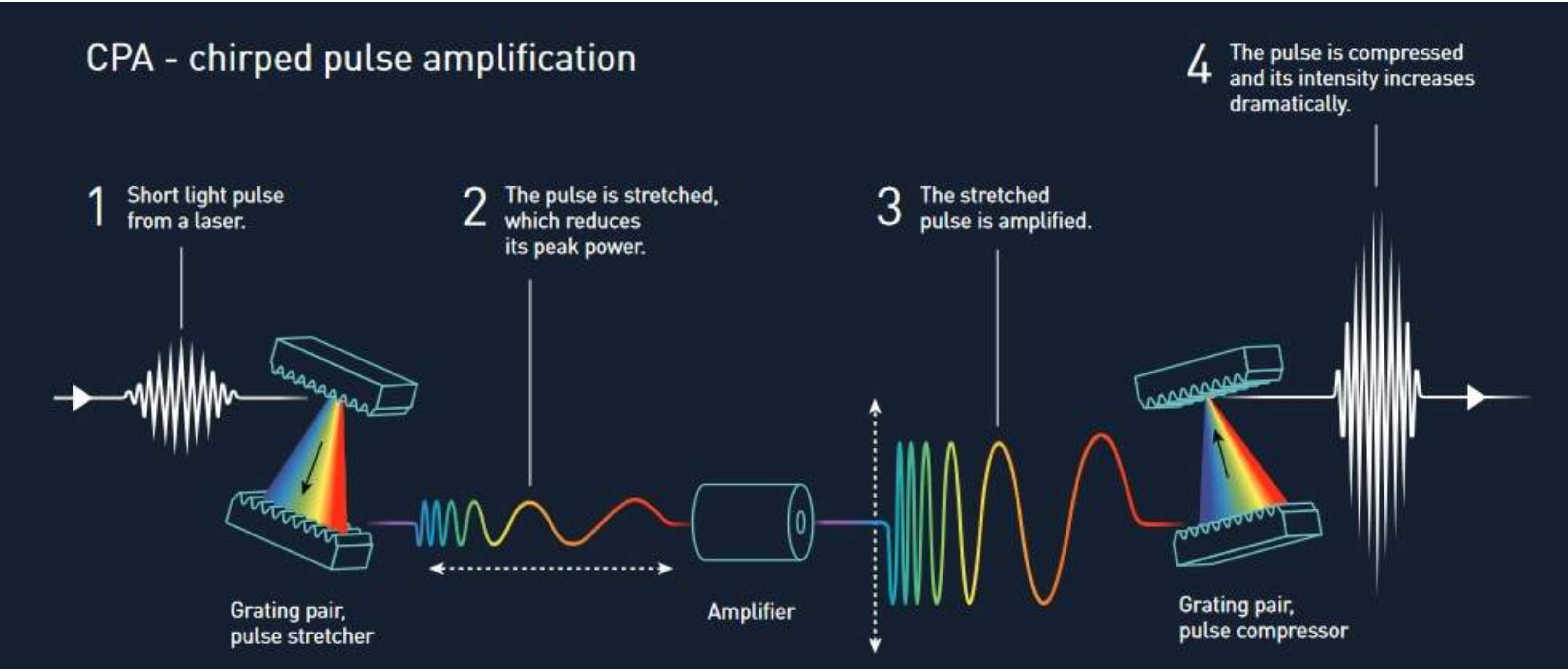

Creating HEDP conditions: Laser pulses

High-peak-power laser facilities world-wide

2009

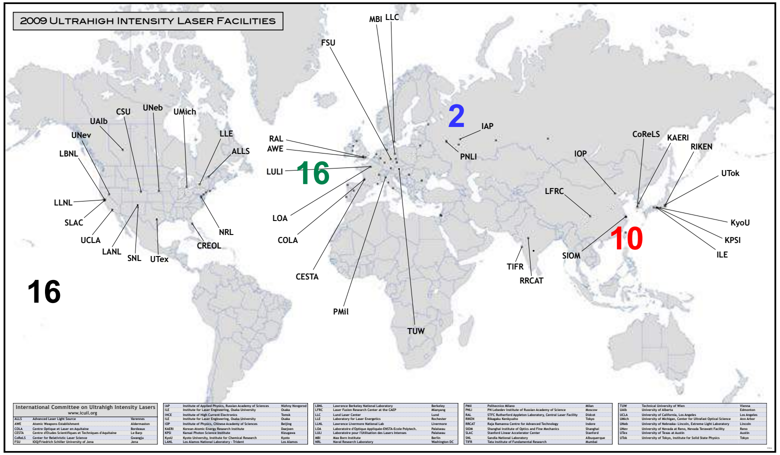

2019

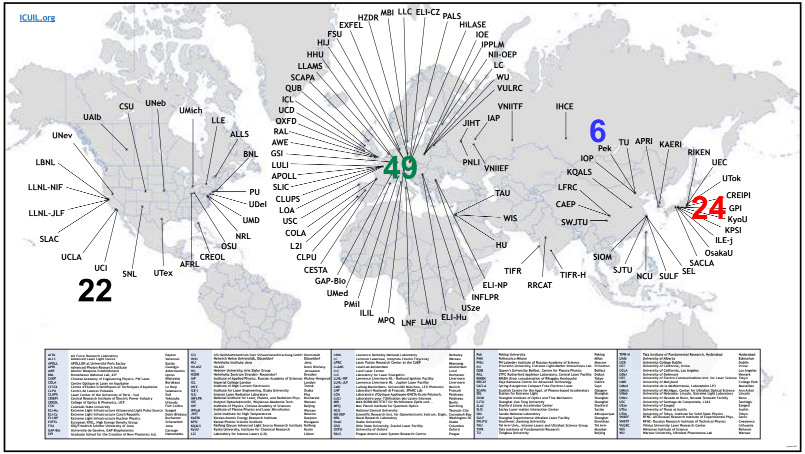

International Committee on Ultra-High Intensity Lasers (ICUIL), https://www.icuil.org/activities/laser-labs.html)

Why study high intensity laser-plasma interactions?

Light pulse

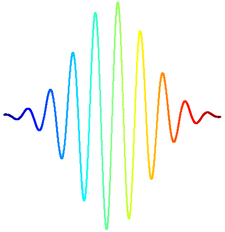

Our “Tool”

Miniaturize accelerators

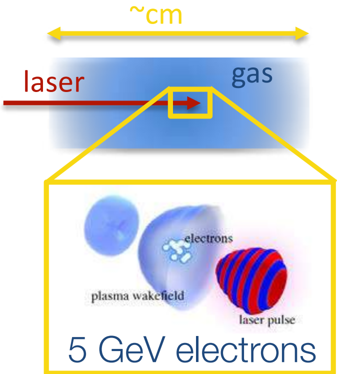

Unique, ultrashort, extremely bright particle & photon sources

Probing basic plasma physics

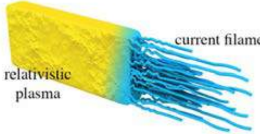

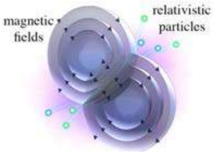

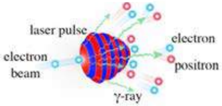

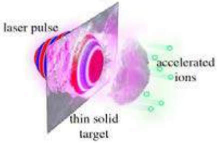

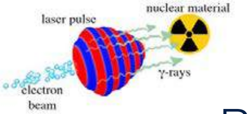

Broader applications…

Laser intensity

Simple definition $\text{Intensity} = \frac{\text{Power}}{\text{Area}} = \frac{\text{Energy}}{\text{Time} \times \text{Area}}$

Example Hercules laser : Energy = 2J
Pulse duration = 40fs
Focal spot radius = 13μm

$\text{Power} = \frac{2}{40 \times 10^{-15}} = 50 \text{ TW}$ 10^{12} (Tera)

$\text{Intensity} = \frac{50 \times 10^{12}}{\pi \times (13 \times 10^{-4})^2} \simeq 10^{19} \text{ Wcm}^{-2}$

↑ in cm

What is high field science?

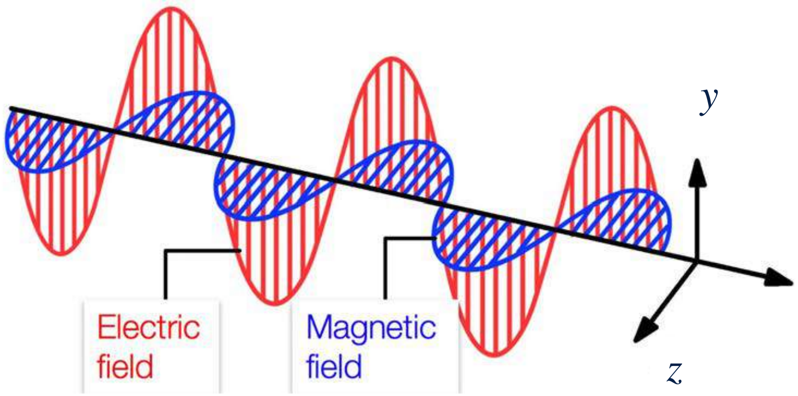

$$\bar{A} = \bar{A}_0 \sin(k_L x - \omega_L t)$$

$$\bar{E} = \frac{\partial \bar{A}}{\partial t} = E_0 \cos(k_L x - \omega t)\hat{y}$$

$$\bar{B} = \nabla \times \bar{A} = B_0 \cos(k_L x - \omega t)\hat{z}$$

Normalized vector potential (normalized field strength)

dimensionless

$$a = \frac{eA}{m_e c} = \frac{eE}{m_e c \omega_L}$$

Interaction of a laser with an electron

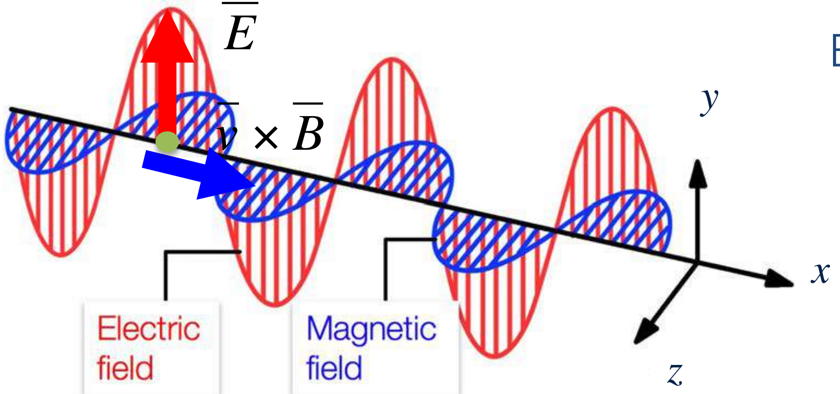

Relativistic regime
$a > 1$

$I = \frac{a_0^2}{\lambda_\mu^2} 1.4 \times 10^{18}\ \mathrm{W cm^{-2}}$ ← in μm

Electron motion in the laser fields:

$$\frac{d\bar{p}_e}{dt} = -e(\bar{E} + \bar{v} \times \bar{B})$$

↑ v → c

$$\frac{p_y}{m_e c} = a = \frac{eE}{m_e c \omega_L}$$

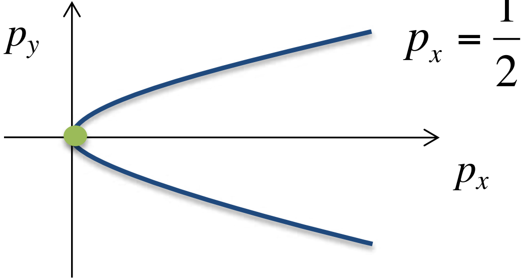

$$p_x = \frac{1}{2} p_y^2$$

$$\frac{p_x}{m_e c} = \frac{a^2}{2}$$

Relativistic electron heating

$$\frac{p_y}{m_e c} = a = \frac{eE}{m_e c \omega_L}$$

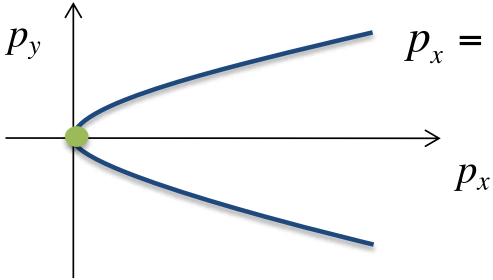

$$p_x = \frac{1}{2} p_y^2$$

$$\frac{p_x}{m_e c} = \frac{a^2}{2}$$

$j \times B$ heating

[Lorentz force $\bar{v} \times \bar{B}$ significant]

Electrons at a sharp interface from underdense to overdense get pushed forward twice every laser period into the overdense plasma → e^-s escape laser fields & gain energy.

$$T_{hot}[keV] \simeq 511 \left(\sqrt{1 + \frac{I \lambda_{\mu}^2}{2.8 \times 10^{18}}} - 1 \right)$$

Laser-plasma generated magnetic fields

Nanosecond pulses, $I \sim 10^{14}$ Wcm^{-2}
$B \sim 1$ MG
$v_B \sim 10^5$ ms^{-1}

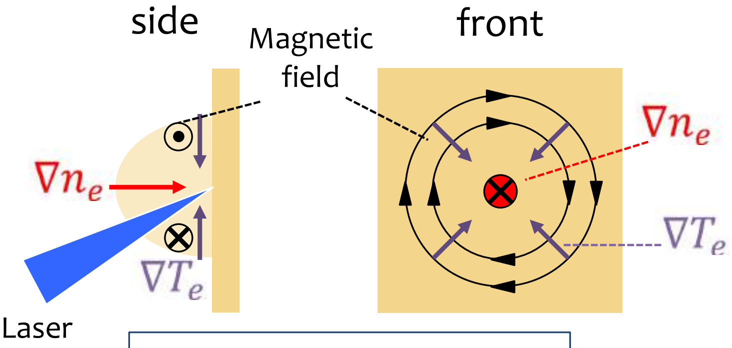

$$\frac{\partial \mathbf{B}}{\partial t} = \frac{k_B}{e n_e} \nabla T_e \times \nabla n_e$$

Picosecond pulses, $I \sim 10^{19}$ Wcm^{-2}
$B \sim 100$ MG
$v_B \sim c$

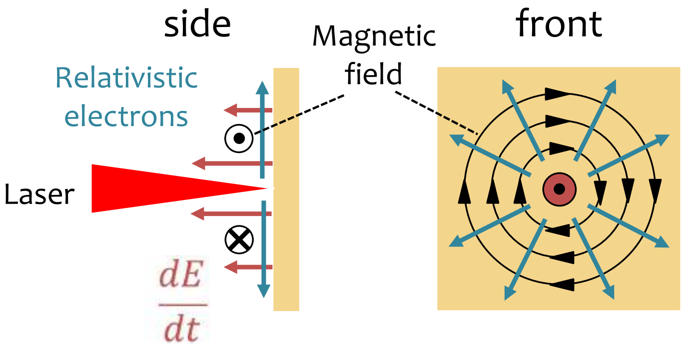

JA Stamper and BH Ripen, PRL, 34, 138 (1975);
CK Li, et al., PRL, 97, 255001 (2006)
L. Gao et al. PRL, 114, 215003 (2015)

W. Schumaker et al. PRL, 110, 015003 (2013)
G. Sarri et al. PRL, 110, 255002 (2013)
A. E. Raymond et al. PRE, 98, 043207 (2018)

Particle-in-cell simulations illustrate the magnetic field generation, dynamics and characteristics for picosecond interactions

1 ps, a_o = 5

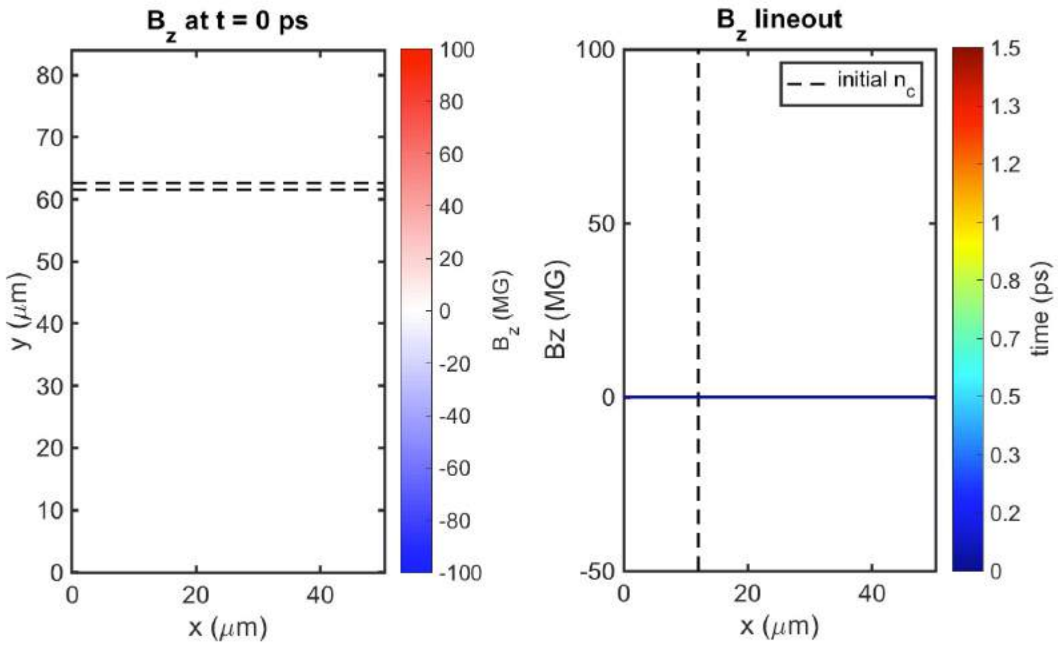

Simulations show the magnetic energy can exceed the rest mass energy to access a new regime in the laboratory

magnetization parameter →

$$\sigma_{cold} = \frac{B^2}{\mu_0 n_e m_e c^2}$$

σ_{cold} → ratio of energy density of B-fields to rest mass energy density

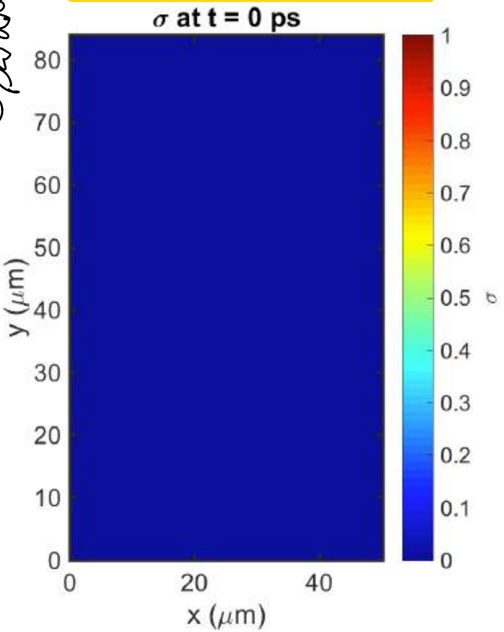

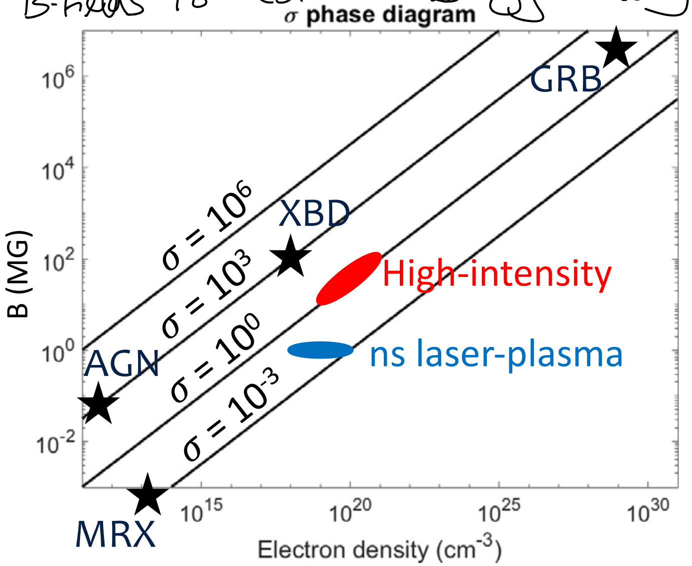

MRX: H Ji and W Daughton, et al., PoP (2011)
XBD: X-ray binary disk coronae

Relativistic electron driven magnetic reconnection is created by focusing 2 laser pulses in close proximity

face on

side on

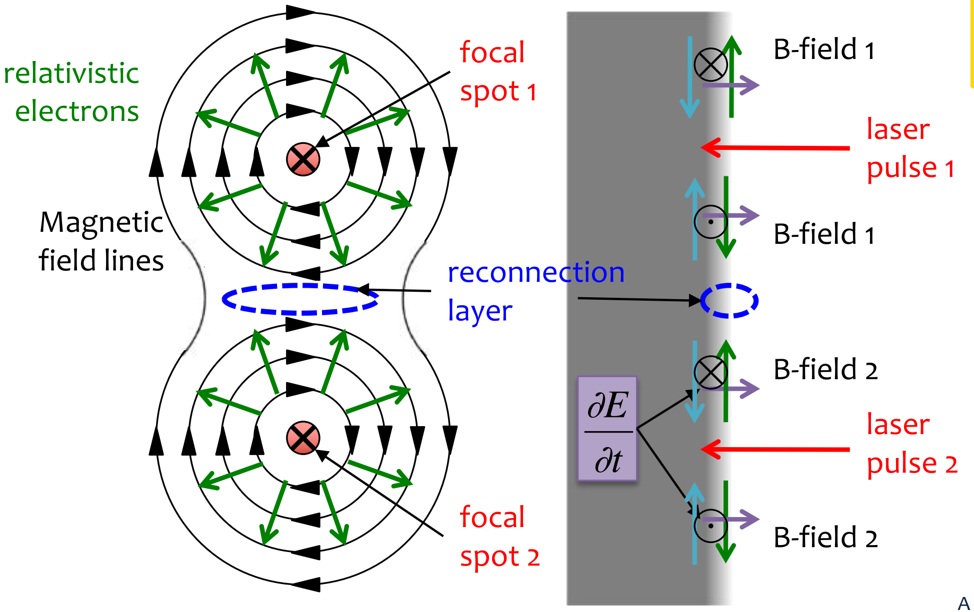

Magnetic field lines are driven together at ~ c

Surface layer has $\sigma_{cold} \geq 1$

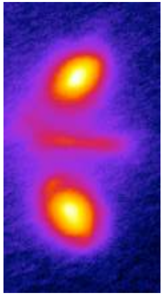

A Raymond, et al., PRE, **98**, 043207 (2018)

Proton probing of a magnetic reconnection geometry at threshold relativistic intensity was performed at Vulcan (RAL)

Charlotte Palmer

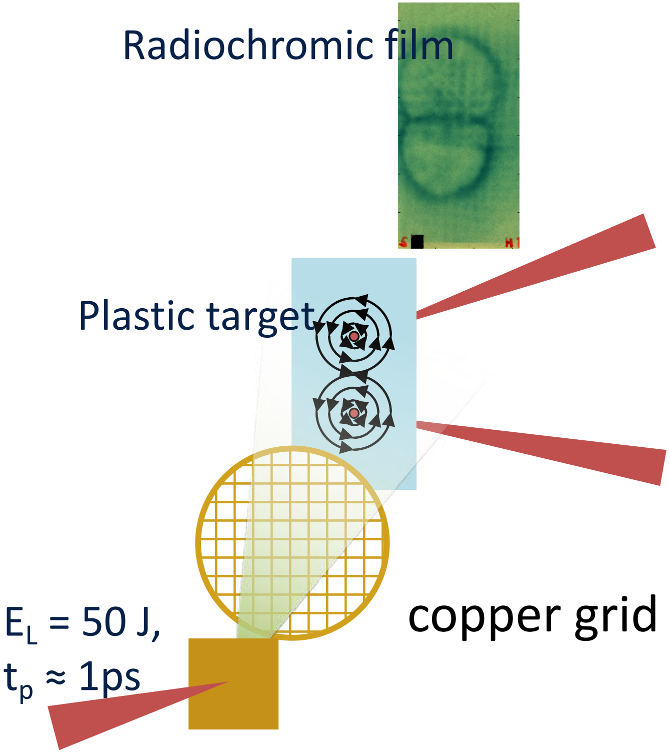

Vulcan Target Area West

Split mirror divides 100 J, 10 ps

I = 7 x 10^{17} Wcm^{-2} per focal spot

Proton probing of a magnetic reconnection geometry at close to threshold intensities was performed at Vulcan (RAL)

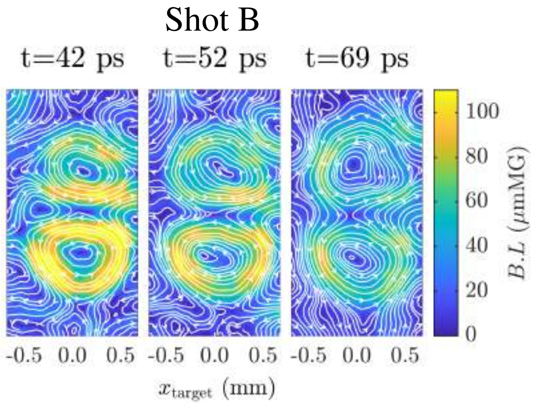

Field decays more rapidly internally than externally
→ could be due to magnetic reconnection

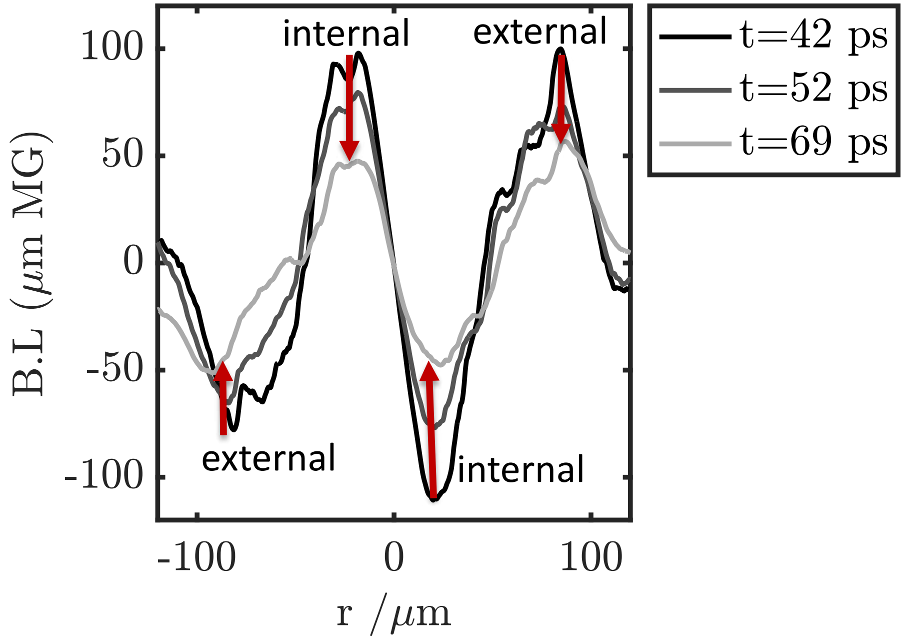

CAJ Palmer, et al., Physics of Plasmas, 26, 083109 (2019)

Laser-driven reconnection experimental setup(s)

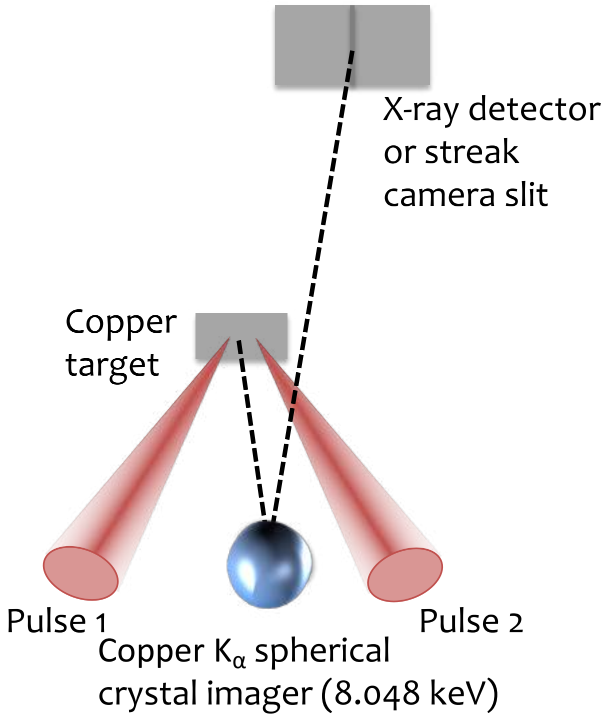

Hercules

2 J, 40 fs

Intensity = 2 x 10^{19} Wcm^{-2}

OMEGA EP

(500 – 1000) J, 20 ps

Intensity = (1.2 – 2.5) x 10^{18} Wcm^{-2}

A Raymond, et al, PRE, 98, 043207 (2018)

The fast electron density closely corresponds to the emitted copper K_α signal

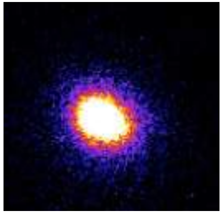

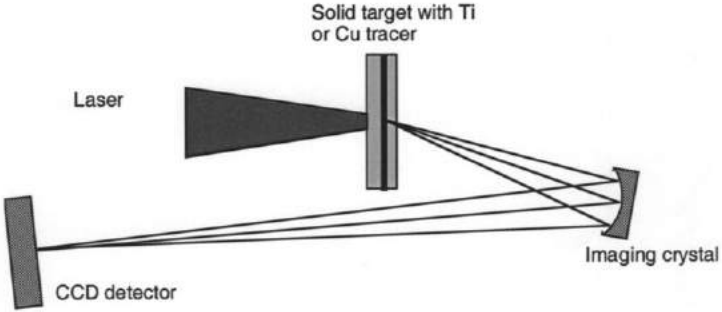

A spherically bent quartz crystal (Q(211) satisfies the Bragg condition in 2nd diffraction order at to form an image with 8.048 keV photons.

JA Koch, et al., RSI, 74, 2130 (2003)

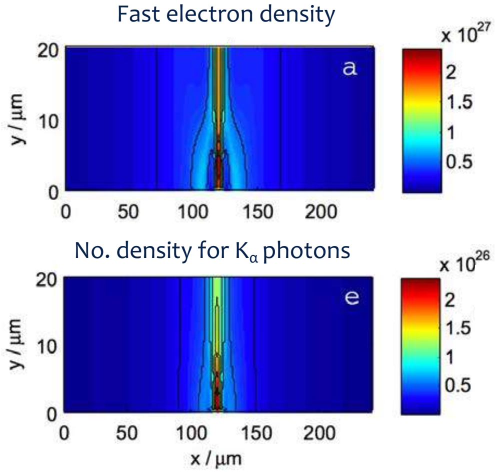

AGR Thomas, et al., NJP, 15, 015017 (2013)

Experimental setup(s)

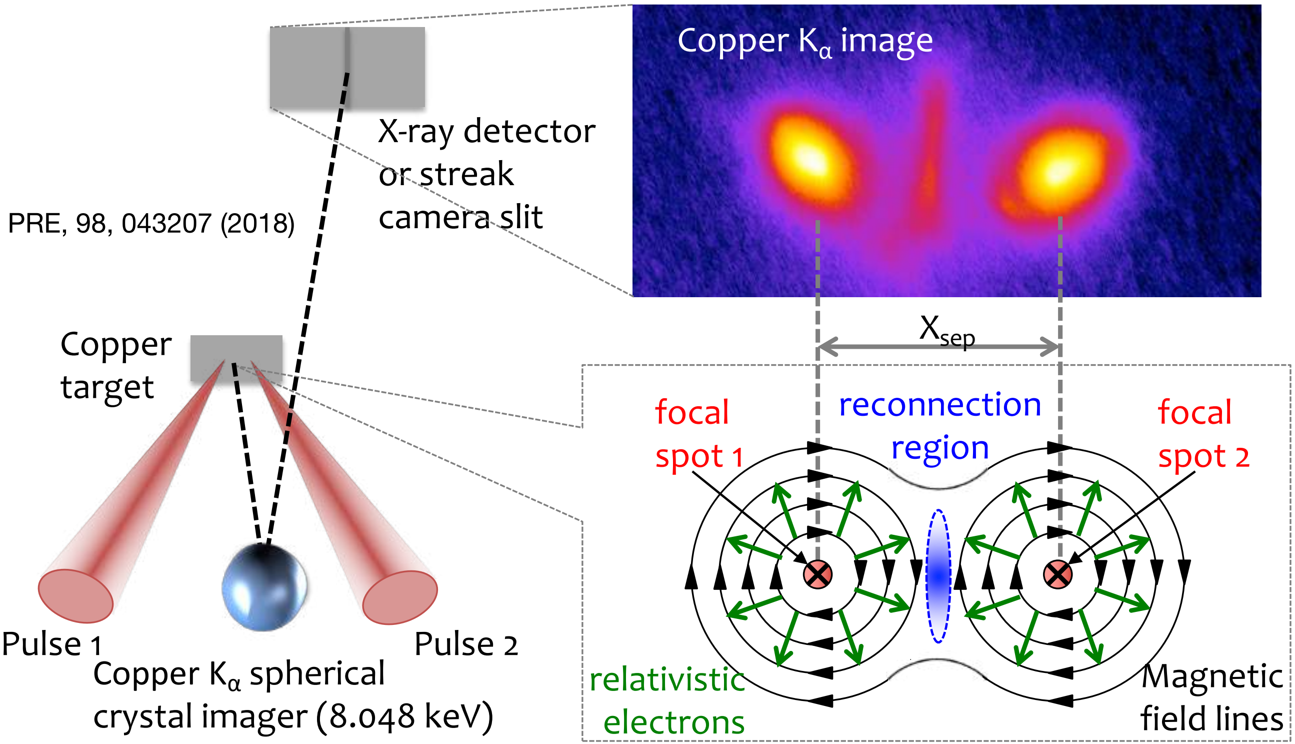

A Raymond, et al, PRE, 98, 043207 (2018)

Magnetic reconnection reconfigures magnetic fields into a lower energy state to release energy and heat the plasma

Reconnection time scale → current sheet aspect ratio, δ/L

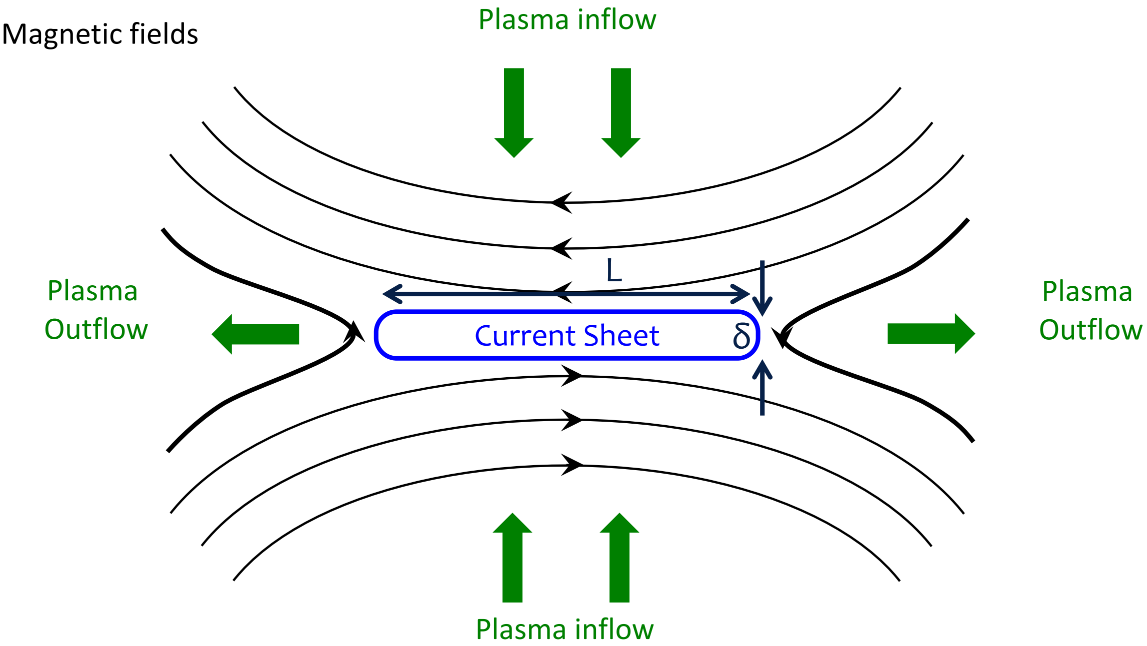

Hercules experiment: Midplane signal appears when both pulses arrive on target together

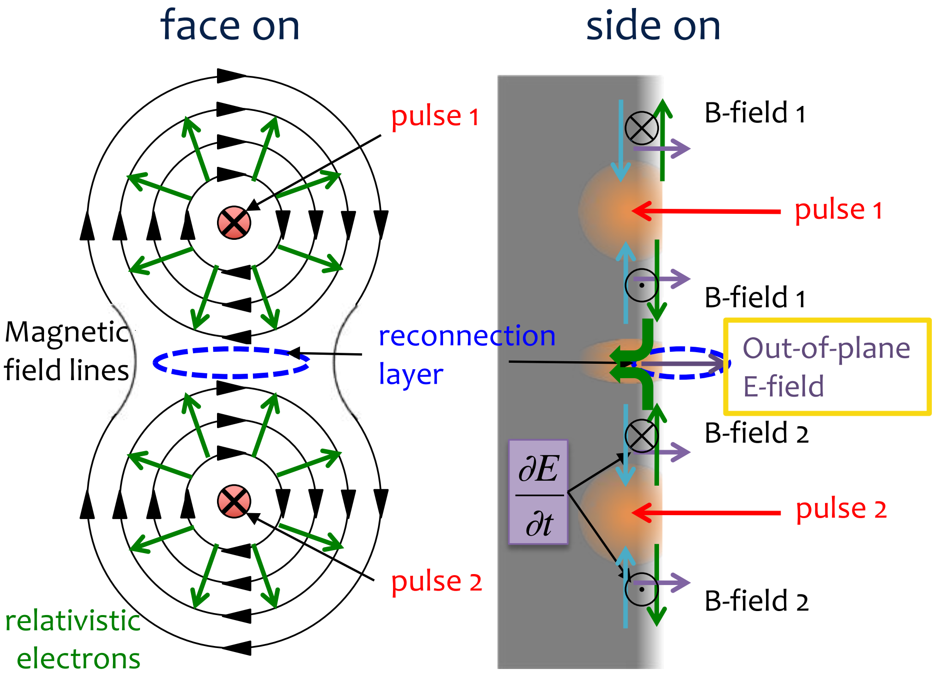

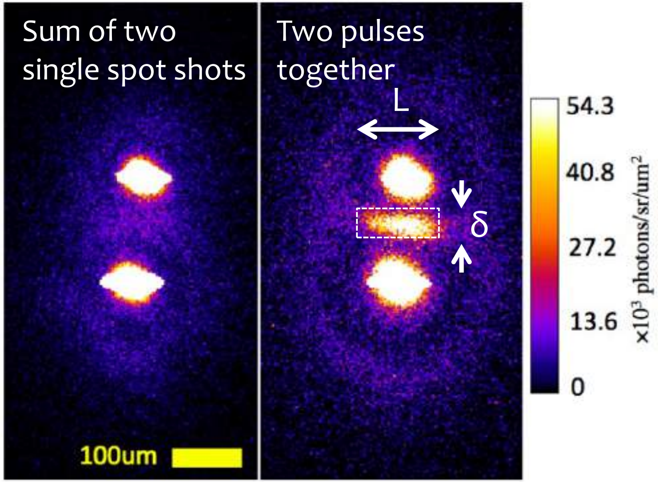

Varying the focal spot separation changed the dimensions of the midplane copper K_α signal

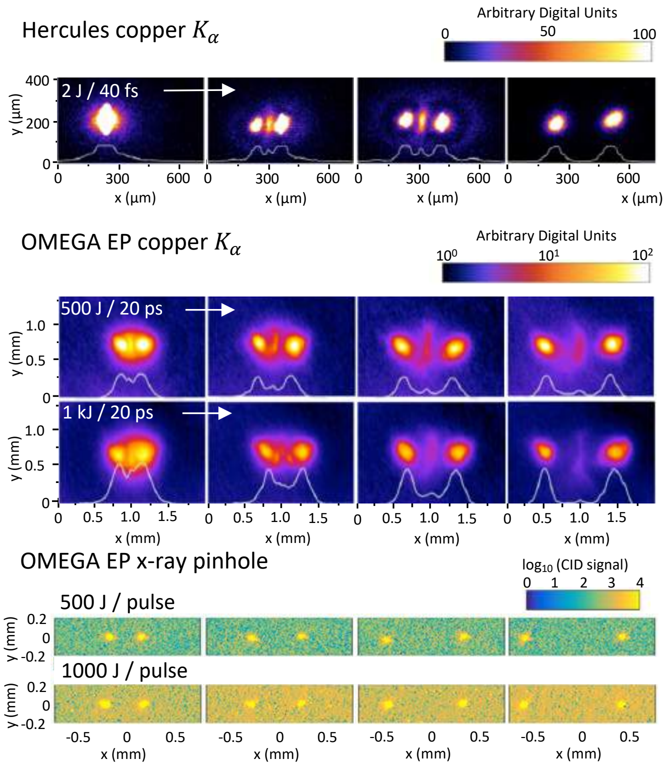

current sheet aspect ratio, $\delta/L \approx 0.3$

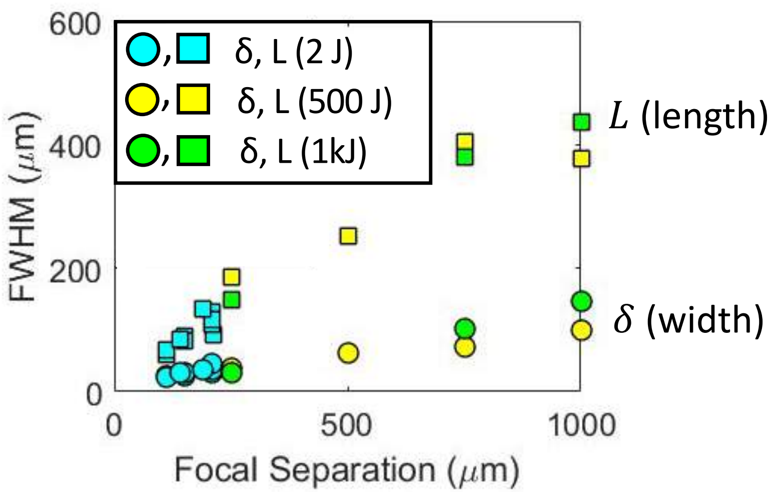

A Raymond, et al, PRE, 98, 043207 (2018)

A modified electron spectrum with a non-thermal population is observed when the laser pulses arrive concurrently on the target

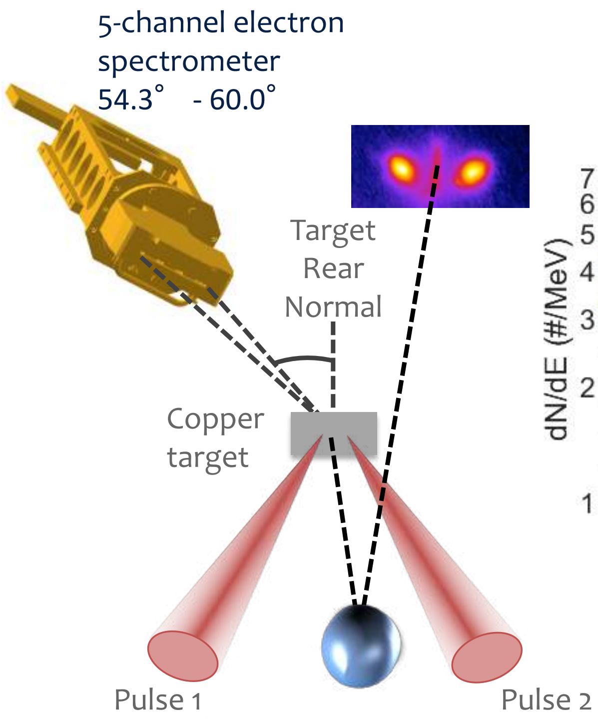

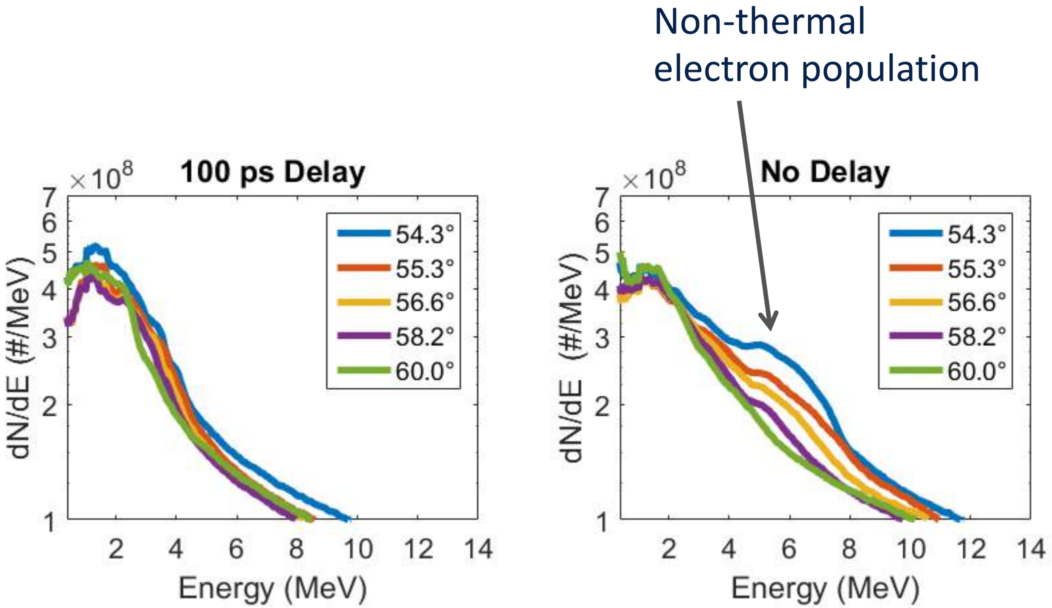

A Raymond, et al, PRE, 98, 043207 (2018)

3D particle-in-cell modeling of a reduced scale system used periodic boundary to form an effective spot separation of 50μm

Run on 25200 nodes of the NASA Pleiades supercomputer

- a_0 = 3, $\tau_p = 20$ fs
- Single pulse with periodic boundary create an effective spot separation of 50 μm

- 40 cells per λ
- 3 x 3 x 3 particles per cell
- n_{max} = 30 n_c
- Plasma scalelength of λ
- Stationary ions

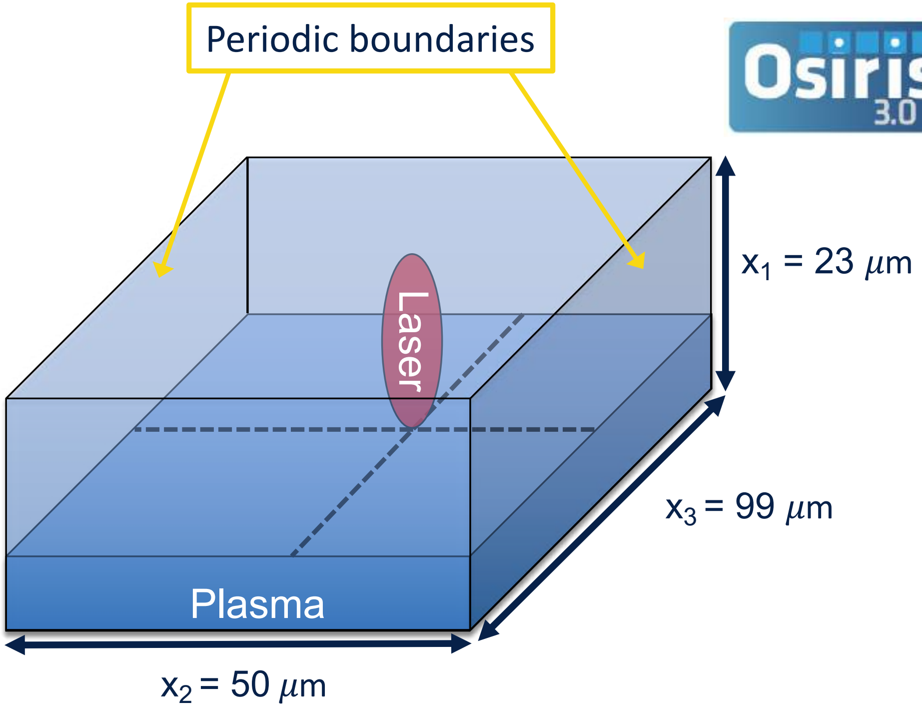

3D PIC shows the formation of the midplane current sheet and associated target normal electric field

Magnetic field lines

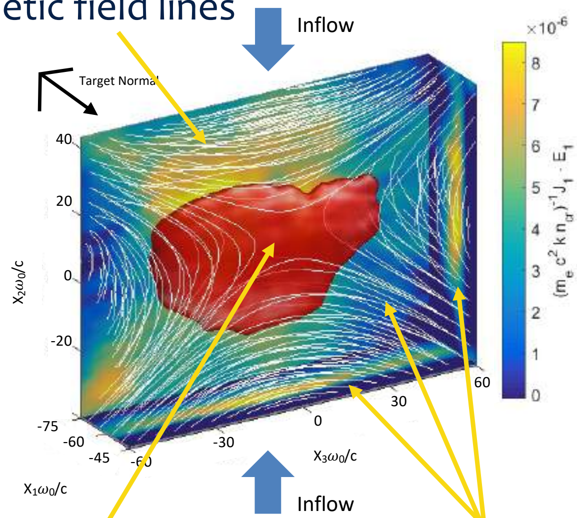

$E_1/cB_{R0} \approx 0.133$

Where $B_{R0} \approx 200$T

$E_1.J_1$ evaluated along central planes

current sheet aspect ratio, $\delta/L \approx 0.3$

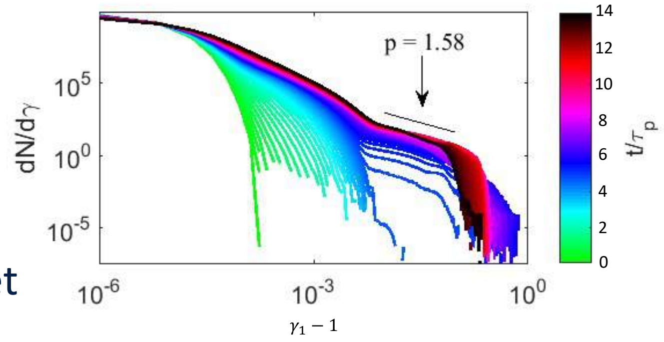

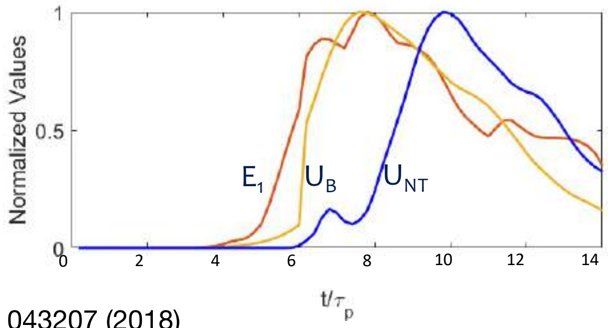

A Raymond, et al, PRE, 98, 043207 (2018)

Can we create a pair plasma in the laboratory?

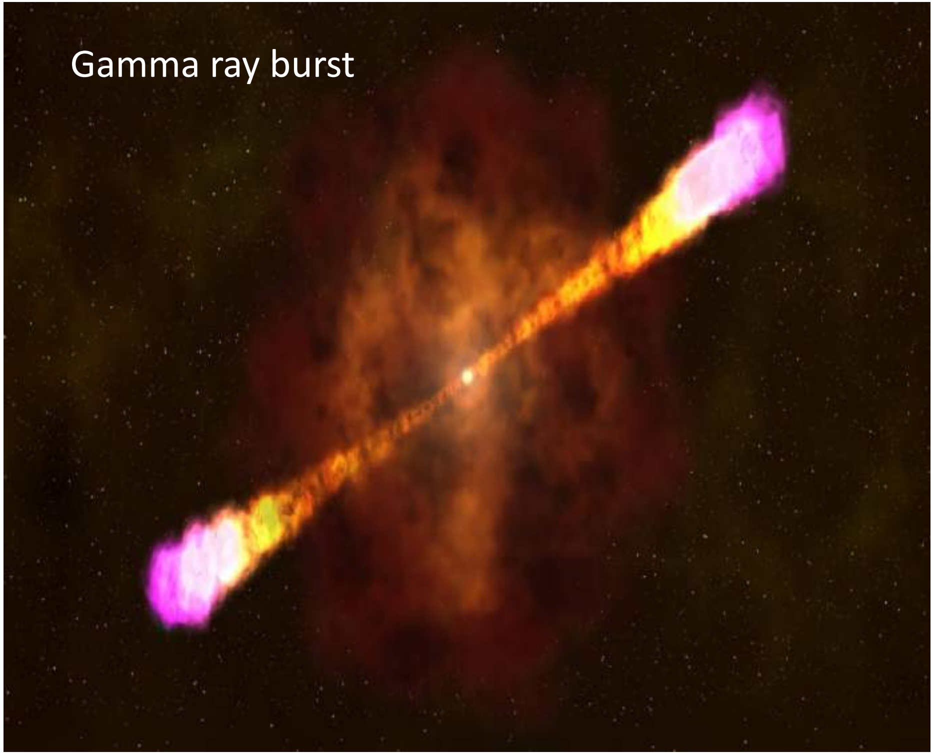

Positrons have the same mass as electrons, but opposite charge.

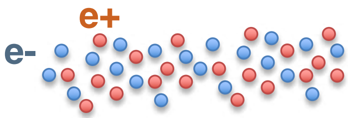

The mass symmetry removes the separation of fast and slow scales present in electron-ion plasmas.

Tsytovich & Wharton (1978) Comments Plasma Phys. Controlled Fusion (1978)

Collisionless shocks of relativistic pair plasma could be drivers of gamma emission.

Liang et al. Scientific Reports (2015) Sarri et al. Nature (2015)

Materials from Hui Chen (LLNL)

Can we create a pair plasma in the laboratory?

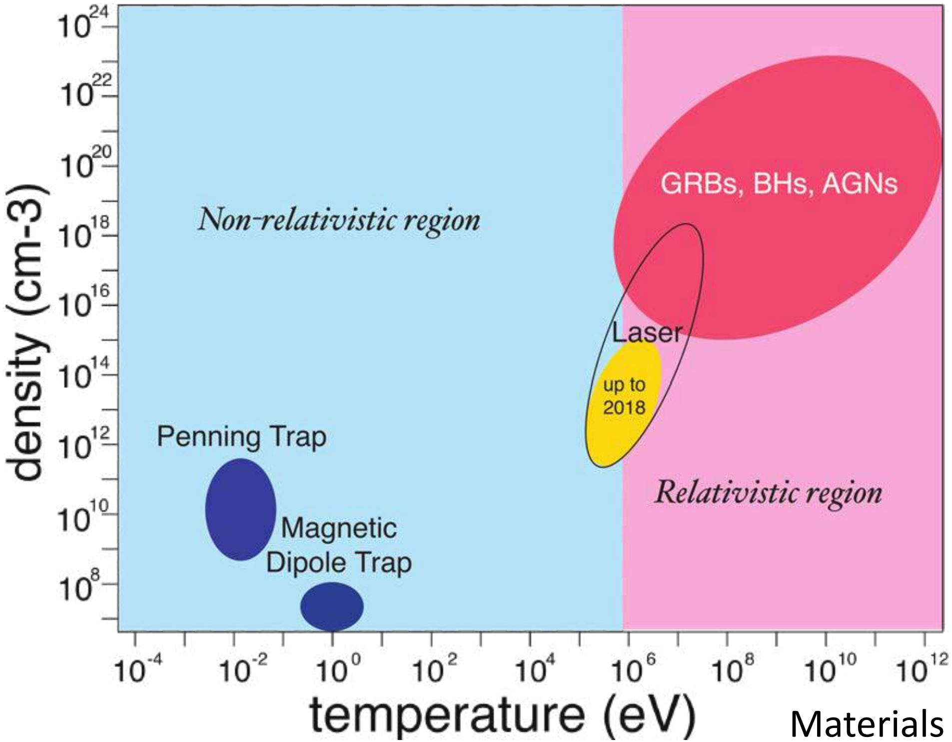

Materials from Hui Chen (LLNL)

Can we create a pair plasma in the laboratory?

Positron generation processes

Trident process

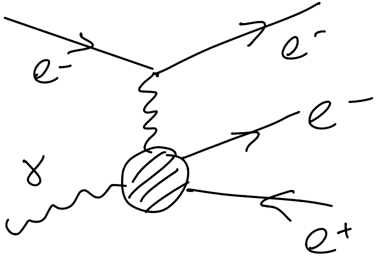

Bethe-Heitler process

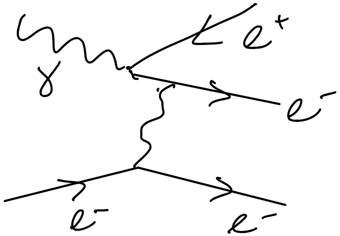

Breit-Wheeler process

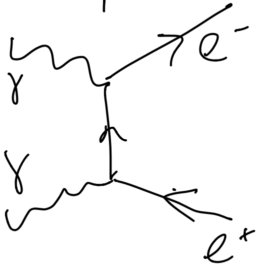

- Need high energy e⁻ & photons
- Generate high-E photons through Bremsstrahlung

Can we create a pair plasma in the laboratory?

Bremsstrahlung (breaking) radiation:

- Strong electric field of the atomic nuclei slows down and deflects an electron
- High Z nuclei have strongest effect
- Photon energies up to the highest energy electrons

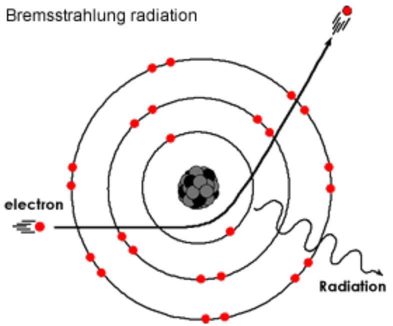

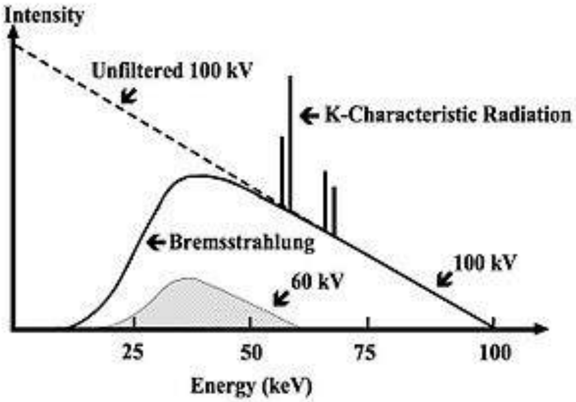

Can we create a pair plasma in the laboratory?

Laser plasma interactions can generate dense, relativistic energy electron beams

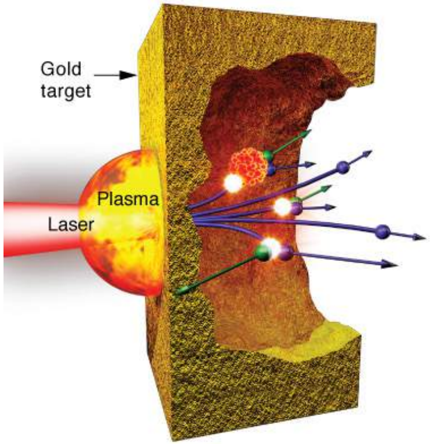

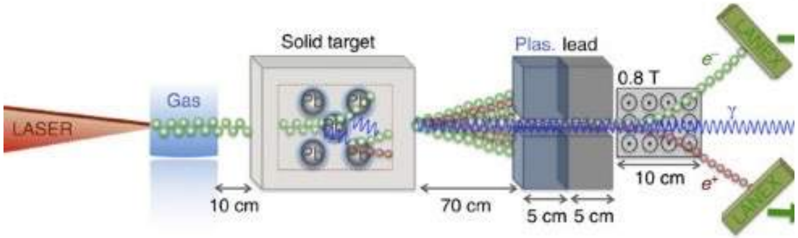

H Chen, et al., PRL, 102, 105001 (2009)

G Sarri, et al., PRL, 110, 255002 (2013)

Can we create a pair plasma in the laboratory?

PRL **114**, 215001 (2015) PHYSICAL REVIEW LETTERS week ending 29 MAY 2015

Scaling the Yield of Laser-Driven Electron-Positron Jets to Laboratory Astrophysical Applications

Hui Chen,[1] F. Fiuza,[1,2] A. Link,[1] A. Hazi,[1] M. Hill,[3] D. Hoarty,[3] S. James,[3] S. Kerr,[4] D. D. Meyerhofer,[5] J. Myatt,[5] J. Park,[1] Y. Sentoku,[6] and G. J. Williams[1]

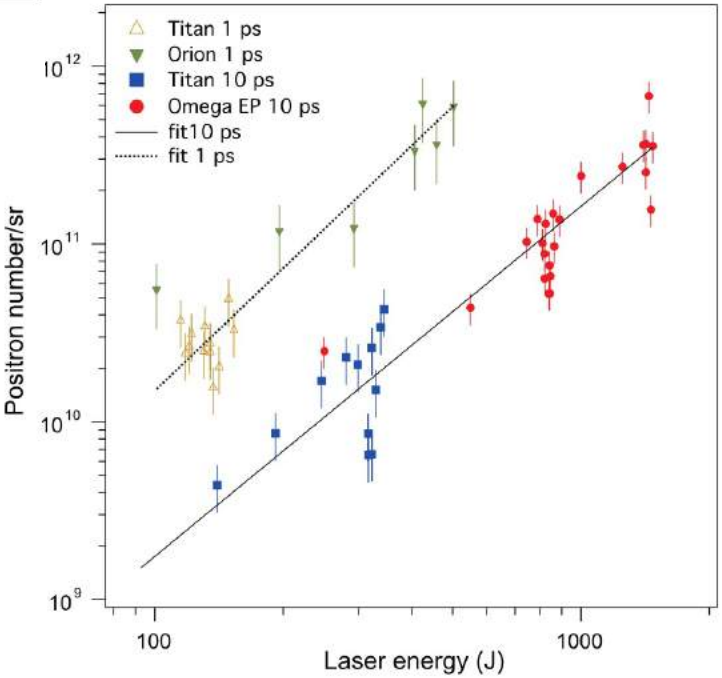

FIG. 1 (color online). Dependence of the measured positron yield on the laser energy, E_L, obtained at three different laser facilities: Omega EP, Orion, and Titan. The upper group is from shots with 1 ps laser pulse: (brown) triangles Titan and (green) diamonds Orion. The lower group is obtained with 10 ps laser pulse: (blue) squares Titan and (red) circles Omega EP.

Can we create a pair plasma in the laboratory?

Requirements to achieve a pair plasma

Debye length < system size

$$\lambda_D^2 = \frac{\epsilon k_B T_e}{n_e e^2}$$

need → large n_e
small $k_B T_e$

System assembled for timescales > process of interest timescale

→ Need to confine pairs → use magnetic mirror

Can we create a pair plasma in the laboratory?

A magnetic pulse power coil focuses the positron beam

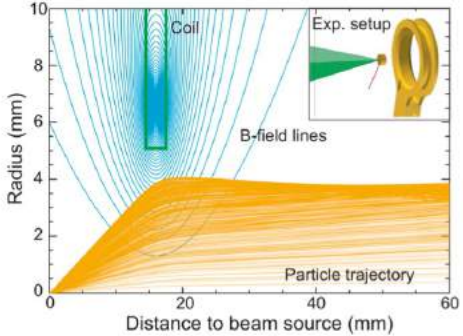

This creates an approaching quasi-neutral jet of pairs

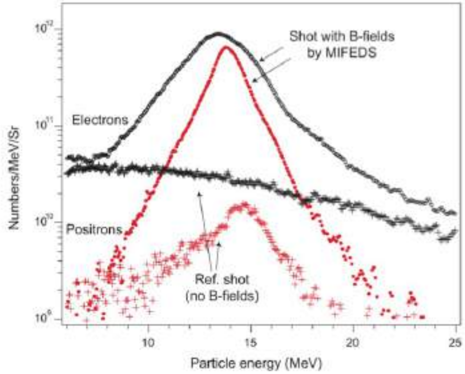

H. Chen, et al, PoP 21, 040703, 2014

Can we create a pair plasma in the laboratory?

Magnetic mirror

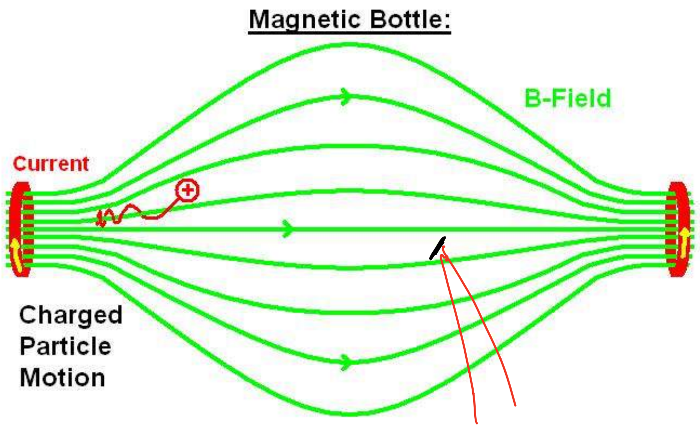

Strong B-field | Weaker B-field | Strong B-field

Assume particle's magnetic moment and total energy don't change→ magnetic moment:

$$\mu = \frac{mv_\perp^2}{2B}$$

In regions of larger B, $v_\perp$ increases

But the total energy must remain constant:

$$\varepsilon = q\phi + \frac{1}{2}mv_\parallel^2 + \frac{1}{2}mv_\perp^2$$

For $\phi = 0$, this means $v_\parallel$ must drop, even go negative.

Particles bounce between coils.

Can we create a pair plasma in the laboratory?

Particle tracking indicates good mirror confinement of < 3 MeV particles

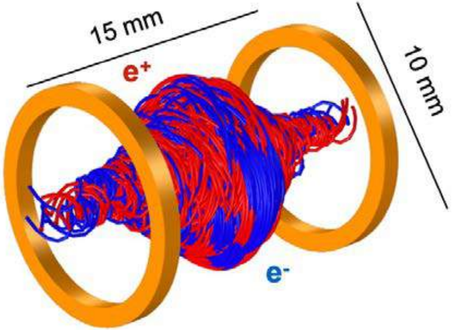

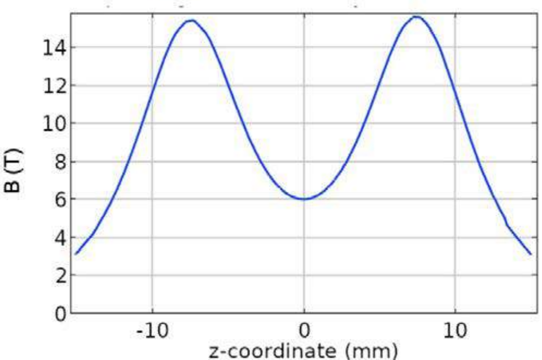

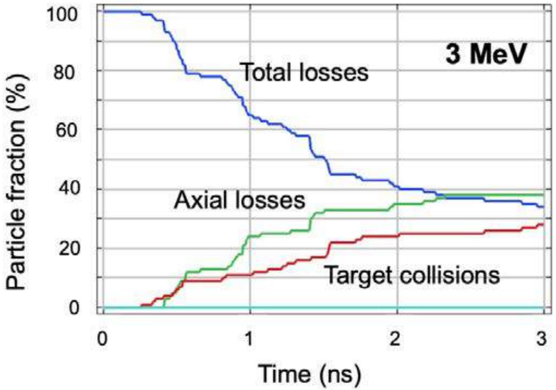

Materials from G Fiksel, et al.

Can we create a pair plasma in the laboratory?

Materials from G Fiksel, et al.

Axial loses increase with magnetic fields on

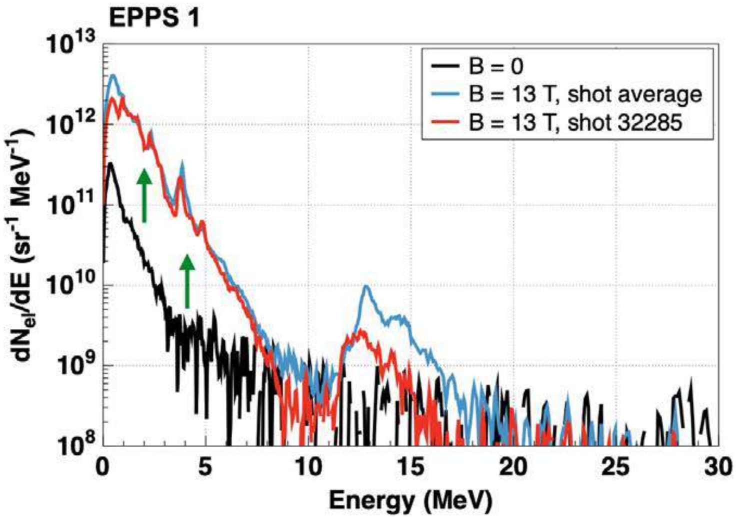

E < 3 MeV are well confined and only are lost axially
Axial flux of 3 MeV < E < 15 < MeV is increased
15 MeV particles are focused by B-field

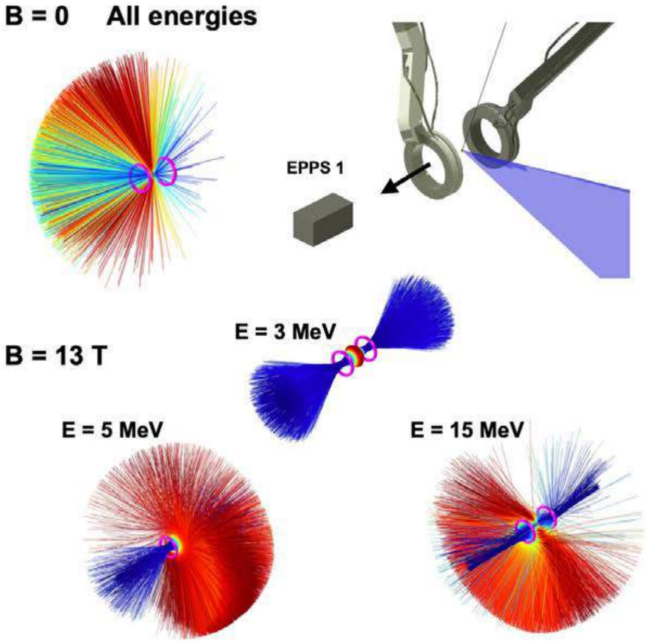

Can we create a pair plasma in the laboratory?

Highest positron yield = 10^{12} positrons

This 13 T magnetic mirror can contain a pairs for times of ~ nanoseconds, with $\gamma \approx 6$ and magnetization $\sigma \approx 40$. The Debye length and skin depth approach unity.

To achieve more significant pair plasma, need:

- To increase positron yield and decrease the average energy of the positrons
- And/or increase the magnetic field (to increase the particle energy that can be trapped)

ZEUS laser facility

ZEUS
Zettawatt-Equivalent Ultrashort Pulse Laser System

Zettawatt $= 10^{21}$ W

Equivalent

Critical field
$E_c \sim 10^{18}$ V/m

Ultrashort pulse laser

System

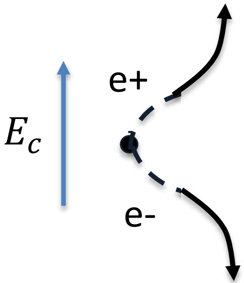

Electric field strength (V/m)

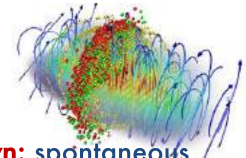

10^{20}

Vacuum breakdown: spontaneous creation of electron-positron pairs

10^{15}

Current laboratory record

Electron accelerated to rest mass energy in 1 μm

10^{10}

Electric field of hydrogen ground state

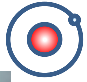

10^{5}

10^{0}

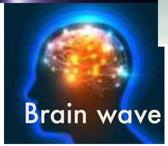

ZEUS laser facility

Zettawatt-Equivalent Ultrashort Pulse Laser System

Zettawatt = 10^{21} W

Equivalent

Critical field
$E_c \sim 10^{18}$ V/m

Ultrashort pulse laser

System

ZEUS power = 3 PW = 3 x 10^{15} W
(Highest power laser in the USA)

In the rest frame of reference, a GeV electron beam the intensity experienced will be equivalent to a Zettawatt power pulse!

10^{22} W/cm^2 laser pulse

GeV electron beam

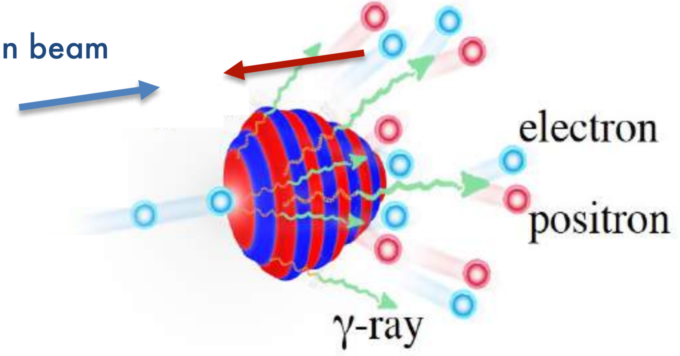

ZEUS laser facility

ZEUS
Zettawatt-Equivalent Ultrashort Pulse Laser System

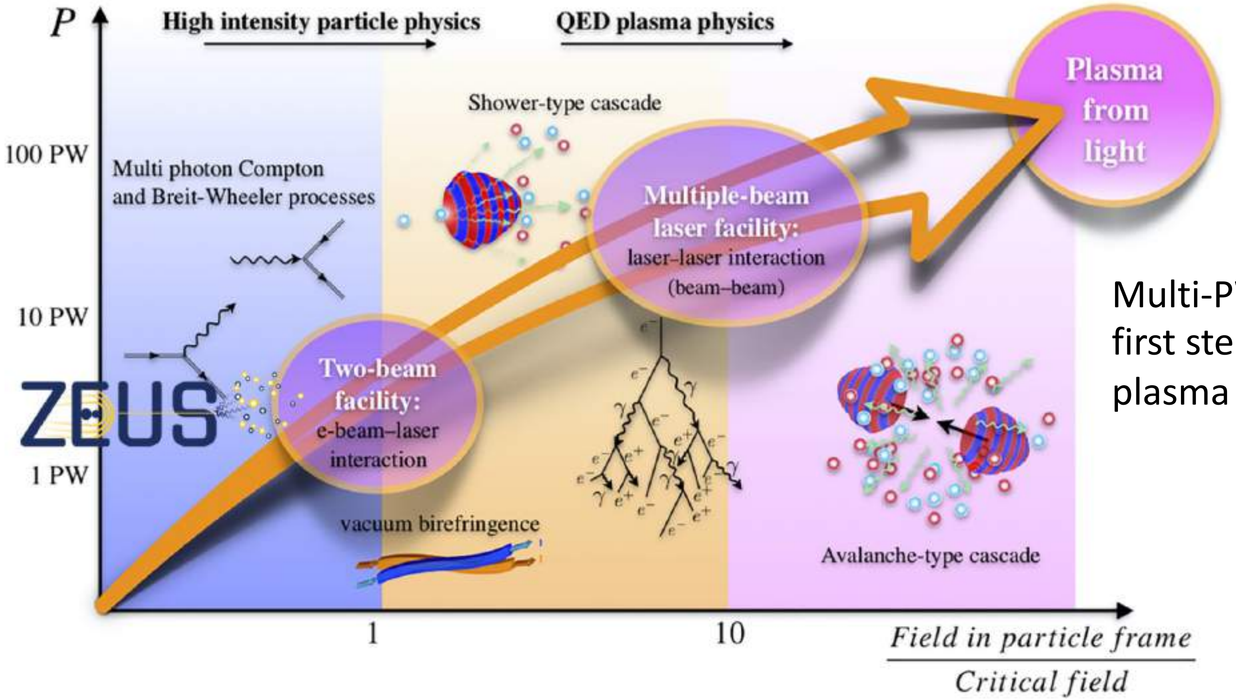

Multi-PW lasers are a first step in generating a plasma from light

Workshop on Opportunities, Challenges, and Best Practices for Basic Plasma Science User Facilities (arXiv:1910.09084)

MICHIGAN ENGINEERING
UNIVERSITY OF MICHIGAN